Hydrogel-Induced Cell Membrane Disruptions Enable Direct Cytosolic Delivery of Membrane-Impermeable Cargo

Jelter Van Hoeck, Thijs Van de Vyver, Aranit Harizaj, Glenn Goetgeluk, Pieterjan Merckx, Jing Liu, Mike Wels, Félix Sauvage, Herlinde De Keersmaecker, Christian Vanhove, Olivier G. de Jong, Pieter Vader, Heleen Dewitte, Bart Vandekerckhove, Kevin Braeckmans, Stefaan C. De Smedt, and Koen Raemdonck*

Intracellular delivery of membrane-impermeable cargo offers unique opportunities for biological research and the development of cell-based therapies. Despite the breadth of available intracellular delivery tools, existing protocols are often suboptimal and alternative approaches that merge delivery efficiency with both biocompatibility, as well as applicability, remain highly sought after. Here, a comprehensive platform is presented that exploits the unique property of cationic hydrogel nanoparticles to transiently disrupt the plasma membrane of cells, allowing direct cytosolic delivery of uncomplexed membrane-impermeable cargo. Using this platform, which is termed Hydrogel-enabled nanoPoration or HyPore, the delivery of fluorescein isothiocyanate (FITC)–dextran macromolecules in various cancer cell lines and primary bovine corneal epithelial cells is convincingly demonstrated. Of note, HyPore demonstrates efficient FITC-dextran delivery in primary human T cells, outperforming state-of-the-art electroporation-mediated delivery. Moreover, the HyPore platform enables cytosolic delivery of functional proteins, including a histone-binding nanobody as well as the enzymes granzyme A and Cre-recombinase. Finally, HyPore-mediated delivery of the MRI contrast agent gadobutrol in primary human T cells significantly improves their T_1-weighted MRI signal intensities compared to electroporation. Taken together, HyPore is proposed as a straightforward, highly versatile, and cost-effective technique for high-throughput, ex vivo manipulation of primary cells and cell lines.

1. Introduction

Intracellular delivery techniques are designed to introduce otherwise cell-impermeable molecules (e.g., small molecules, peptides, proteins, nucleic acids, ...) into the cytoplasm, enabling us to guide cell fate, probe cell function, and reprogram cell behavior.[1] As such, intracellular delivery not only contributes to our fundamental understanding of cell biology, but also allows to create new or improve existing therapeutic strategies.

A wide variety of cargo and target cell types can be envisioned, both for in vitro, in vivo, and ex vivo applications.[1,2] In particular, ex vivo cell engineering entails specific needs regarding intracellular delivery approaches.[2] Decades of clinical experience have shown that ex vivo culturing of cells comes with risks of inducing undesired geno- and phenotypic alterations, for instance, the loss of cytokine production or even exhaustion of the proliferative potential of adoptive cell therapies.[3,4] As such, minimizing the time in culture

Dr. J. Van Hoeck, Dr. T. Van de Vyver, Dr. A. Harizaj, Dr. P. Merckx, Dr. J. Liu, M. Wels, Dr. F. Sauvage, Dr. H. De Keersmaecker, Dr. H. Dewitte, Prof. K. Braeckmans, Prof. S. C. De Smedt, Prof. K. Raemdonck
Ghent Research Group on Nanomedicines
Laboratory of General Biochemistry and Physical Pharmacy
Faculty of Pharmaceutical Sciences
Ghent University
Ottergemsesteenweg 460, Ghent 9000, Belgium
E-mail: Koen.Raemdonck@UGent.be
G. Goetgeluk, Prof. B. Vandekerckhove
Department of Diagnostic Sciences
Ghent University
Corneel Heymanslaan 10, Ghent 9000, Belgium
Dr. H. De Keersmaecker, Prof. K. Braeckmans, Prof. S. C. De Smedt
Centre for Advanced Light Microscopy
Ghent University
Ottergemsesteenweg 460, Ghent 9000, Belgium

The ORCID identification number(s) for the author(s) of this article can be found under https://doi.org/10.1002/adma.202008054.

Prof. C. Vanhove
Infinity Lab
Medical Imaging and Signal Processing Group-IBiTech
Faculty of Engineering and Architecture
Ghent University
Corneel Heymanslaan 10, Ghent 9000, Belgium
Prof. O. G. de Jong, Prof. P. Vader
CDL Research
Division LAB
UMC Utrecht
Faculty of Medicine
Utrecht University
Heidelberglaan 100, Utrecht 3584 CX, The Netherlands
Prof. O. G. de Jong
Department of Pharmaceutics
Utrecht Institute for Pharmaceutical Sciences (UIPS)
Faculty of Science
Utrecht University
Universiteitsweg 99, Utrecht 3584 CG, The Netherlands

is vital, requiring high-throughput delivery techniques that offer high delivery efficiencies while maintaining a high cell viability.[5–7] In addition, many applications (e.g., differentiation of stem cells) require an ideal combination of small molecules and macromolecular cargo to be delivered, demanding highly flexible delivery techniques.[1,8–11] Finally, with regard to fundamental research and even more so the scale-up of cell therapies, cost-effective and straightforward delivery methods are needed.[12]

Intracellular delivery techniques can be divided into two major categories, that is, membrane-disruption and carrier-based delivery methods.[2] Membrane disruption-mediated delivery typically requires an external physical (e.g., mechanical, electrical, thermal, optical) or chemical (e.g., oxidants, pore-forming agents) trigger to transiently permeabilize the cell membrane. These methods generally offer great flexibility, allowing efficient cytosolic delivery of cargo with divergent physicochemical properties in a wide variety of cell types. However, the need for external stimuli generally requires specialized instrumentation. In addition, the generation of membrane defects is often associated with a substantial loss of cell viability and the induction of undesirable cellular stress responses.[1,13,14]

Carrier-based delivery relies on nanoparticles to package and deliver membrane-impermeable cargo into cells. In general, both viral and non-viral delivery nanocarriers can be distinguished. Due to their high efficiency, viral vectors belong to the most clinically advanced delivery carriers for nucleic acid delivery. They are designed to exploit specific viral infection pathways to enter and transduce target cells. However, the manufacturing process of viruses is costly, labor-intensive, and difficult to standardize. In addition, their use generally comes with multiple safety concerns in vivo, often complicating clinical application.[7,15,16] Non-viral nanocarriers typically make use of (semi-)synthetic materials (e.g., polymers, lipids, inorganic nanomaterials) that either electrostatically complex or physically entrap their (charged) cargo.[17] The ability of non-viral carriers to protect cargo from degradation and target specific tissues, as well as their scalability makes them attractive options for both in vivo and ex vivo delivery applications.[18–20] Nevertheless, cargo encapsulation is generally dependent on the physicochemical properties of both the carrier and the cargo, limiting cargo flexibility compared to membrane disruption-based methodologies. As for most viruses, non-viral carriers also typically enter cells via one or more endocytic pathways depending on their physicochemical properties and the type of cell surface interaction. These pathways are often ill-defined and cell type dependent, complicating widespread use.[21] Furthermore, since endosomal content is prone to rapid recycling toward the cell surface or lysosomal degradation, efficient endosomal[22–24] or lysosomal escape[25,26] strategies are required for cytosolic cargo delivery. Multiple escape mechanisms have been evaluated (e.g., based on endosomal membrane fusion or disruption), but to date remain largely inefficient.[27–30] In addition to these hurdles, sufficient and timely cargo release from the nanocarrier following endocytosis remains a major bottleneck limiting intracellular delivery efficiency.
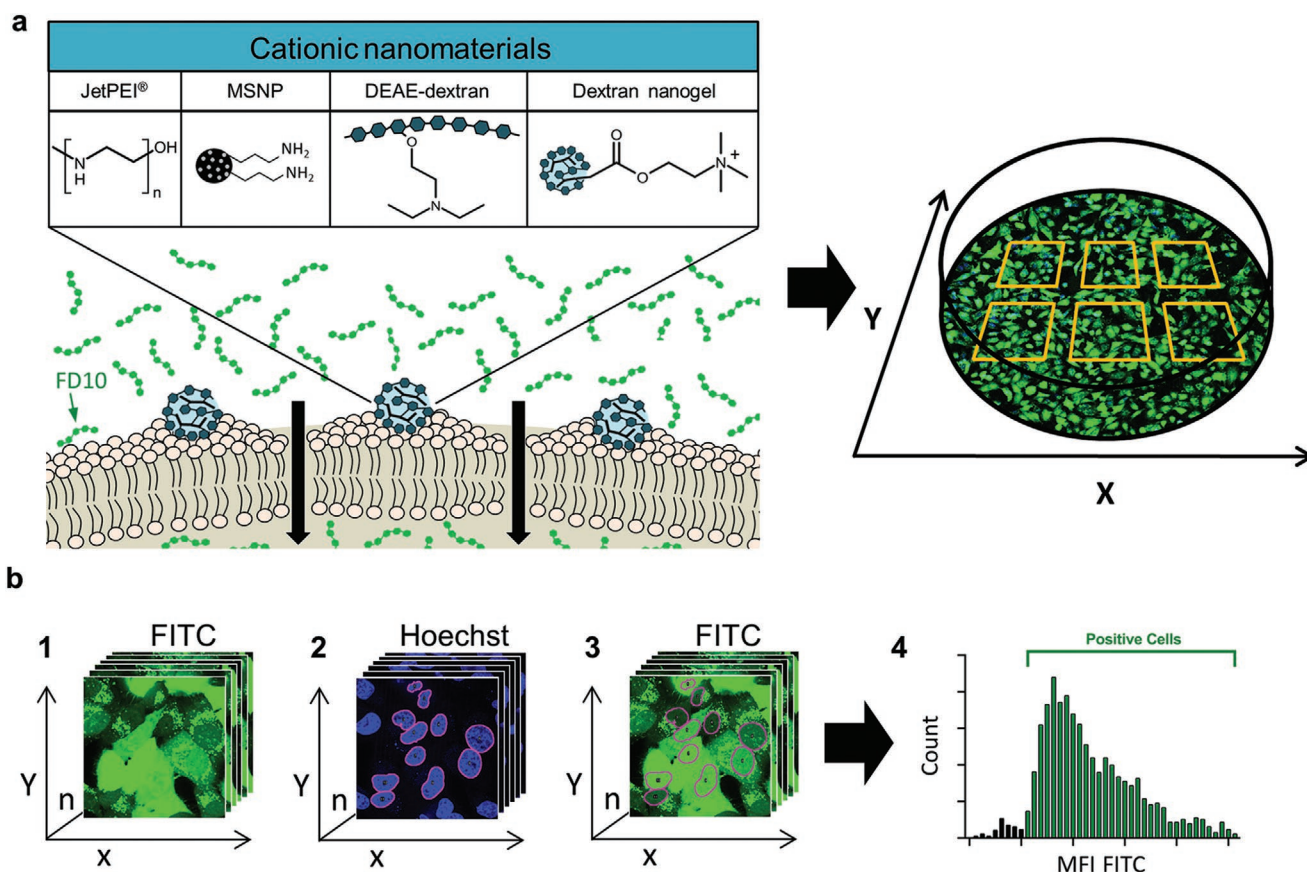
Polycationic materials, such as cationic liposomes and polymers, have been extensively researched for complexation of polyanionic molecules such as nucleic acids into nanoparticles.[31]

Furthermore, they have been shown to internalize more efficiently into cells than their negatively charged counterparts, owing to the electrostatic interaction with the negatively charged cell membrane.[32–34] Notably, multiple studies have shown that commonly used cationic polymers (e.g., diethylaminoethyl (DEAE)-dextran, polyethyleneimine (PEI), polyamidoamine (PAMAM)-dendrimers) and cationic nanoparticles (e.g., surface-modified mesoporous silica nanoparticles and gold nanoparticles) can also induce membrane disruption events such as increased membrane fluidity, membrane thinning, and the formation of nanoscale holes, even at non-toxic concentrations.[34–41] Remarkably, studies using supported lipid bilayers as model membranes revealed that localized membrane thinning events typically precede the complete removal of lipids,[35] eventually resulting in membrane pores with an estimated average size of 15–40 nm in diameter.[37] In addition, theoretical studies have shown these pore formation events to be thermodynamically feasible.[35–37,42,43] Practical evidence for increased cell permeability was mainly provided by showing the influx of small membrane-impermeable molecules (e.g., fluorescent dyes and ions) in viable, polycation-treated cells.[34,36,43,44]

Given the aforementioned studies, we hypothesized that cationic polymers and nanoparticles could not only function as carrier-mediated delivery devices, but could also be positioned as membrane-disruptive agents to enable direct cytosolic delivery of membrane-impermeable compounds. As such, important bottlenecks such as inefficient cargo decomplexation and endosomal escape can be circumvented. Nevertheless, despite the clear experimental proof of extensive but transient membrane perturbations evoked by polycations, the exploitation of this specific functionality for cytosolic cargo delivery remains largely unexplored to date. In this report, we investigated in detail whether polycations can induce nanoscale membrane defects that enable the passage of soluble, freely diffusing, membrane-impermeable molecules directly into the cytosol. After screening several cationic nanoparticles and polymers, we show that crosslinked cationic hydrogel nanoparticles, in contrast to cationic polymers, can effectively permeabilize the plasma membrane of HeLa cells without excessive cell damage, allowing highly efficient cytosolic delivery of FITC-dextran (FD) molecules of up to 40 kDa in molecular weight. Furthermore, we demonstrated successful macromolecule delivery into primary cells such as human T cells and bovine corneal epithelial cells, indicating the broad applicability of this approach for hard-to-transfect cells as well adherent and suspension cells. Finally, as a first functional proof-of-concept, we convincingly showed the cytosolic delivery of several proteins such as a histone-binding nanobody and the enzymes granzyme A and Cre-recombinase, in HeLa cells. Secondly, we describe successful intracellular delivery of the MRI contrast agent gadobutrol in primary human T cells, which further underscores the broad range of applications for which this technology can be used.

2. Screening Polycationic Materials for Cytosolic Delivery of Macromolecules

Polycationic materials have been shown to induce lipid membrane defects, including the formation of nanosized pores.[34–36,44]

Figure 1. Schematic representation of the experimental procedure and quantitative analysis to identify polycationic materials with cytosolic macromolecule delivery capacities. a) HeLa cells were incubated for 2 h with a selected polycationic material in the presence of green fluorescent FITC-Dextran (FD10). Cell nuclei were stained with Hoechst and multiple confocal images were taken. b) Image acquisition was performed using a 408 nm and 488 nm laser line resulting in fluorescence intensity in the blue (Hoechst) and green (FITC) channel (1 and 2). Following nuclei detection in the blue channel (2), a nuclear region of interest (ROI) was determined (3), in which the FITC signal was measured and plotted in frequency distributions for at least 200 cells per condition (4). Based on these histograms, a population of positive cells containing nuclear FD10 was determined. The relative mean fluorescence intensity (rMFI) was calculated as the nuclear MFI for a given condition divided by the nuclear MFI measured in the negative control (only FD10, without a cationic nanomaterial) and this rMFI value was used as an indicator for cytosolic FD10 delivery. MSNP, propylamine-functionalized mesoporous silica nanoparticles; DEAE, diethylaminoethyl; dextran nanogels, dextran methacrylate (MA)-co-TMAEMA nanogels; FD10, FITC-dextran 10 kDa.

To investigate whether these membrane defects could be used for the direct cytosolic entry of membrane-impermeable macromolecules, we tested four commonly used polycationic materials for which the induction of membrane perturbations has been described in the literature,[34,35,38,44] that is, two cationic polymers (linear polyethyleneimine (JetPEI) and DEAE-dextran) and two cationic nanoparticles (propylamine-functionalized mesoporous silica nanoparticles (MSNPs) and a cationic dextran hydrogel nanoparticle (dextran nanogel)). The experimental procedure to quantify cytosolic delivery is illustrated in **Figure 1**. First, HeLa cells were exposed to combinations of the indicated polycationic material at subtoxic concentrations (cell viability ±80%, Figure S1, Supporting Information) and neutral FITC-labeled dextran with an average molecular weight of 10 kDa (FD10), used as a model macromolecule. As (fluid phase) endocytosis of cargo typically leads to its endo-lysosomal sequestration, we adopted a quantification method that allows us to distinguish effective cytosolic FD10 delivery from endocytic uptake. Since cytosolic FD10 can diffuse into the nucleus,

FD10 delivery efficiency was determined based on fluorescence intensity levels measured in the nuclear region of each individual cell using rapid spinning disk confocal imaging. As such, possible interference arising from endo-lysosomal FD10 fluorescence can be avoided.

Bright green punctae are visible in HeLa cells exposed to FD10, indicative of endosomal entrapment following spontaneous pinocytic uptake (**Figure 2**a). In addition, these punctae are more pronounced following co-incubation with cationic nanoparticles, possibly demonstrating increased endocytic uptake as a result of nanoparticle–membrane binding. In strong contrast to the cationic polymers JetPEI and DEAE-dextran, only exposure of HeLa cells to the cationic nanoparticles (MSNPs and dextran nanogels) also caused a marked diffuse staining of the cell cytoplasm and nucleus, indicating successful cytosolic FD10 delivery. However, upon quantifying nuclear FITC fluorescence intensity, dextran nanogels emerged as a far superior polycationic material for cytosolic delivery, showing significantly higher FD10 delivery efficiency (≈90% positive cells, with

ADVANCED
SCIENCE NEWS

www.advancedsciencenews.com

ADVANCED
MATERIALS

www.advmat.de
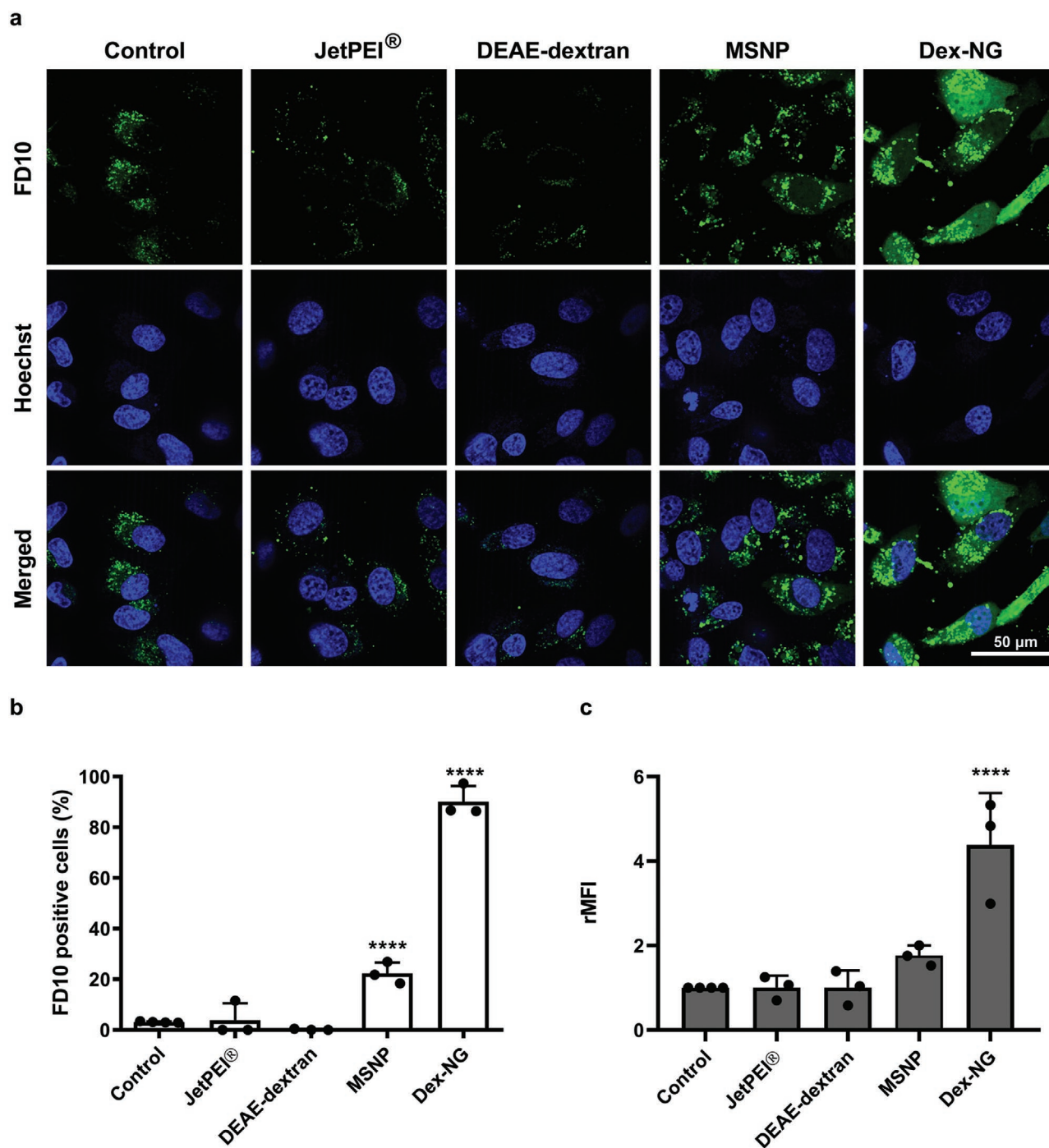
Figure 2. Dextran nanogels efficiently deliver macromolecules in HeLa cells. a) Representative confocal images of FITC-dextran 10 kDa (FD10) delivery in HeLa cells, incubated for 2 h with the indicated polycationic material in Opti-MEM. Green punctae seen in the cytoplasm are indicative for FD10 molecules trapped in endosomes. A diffuse cytosolic and nuclear staining corresponds with free cytosolic FD10. b,c) Quantitative analysis of FD10 delivery in HeLa cells based on nuclear FITC fluorescence intensity, as previously described (>200 cells were imaged and analyzed per condition). Data represent mean ± SD of at least three independent experiments ($n = 4$ for control, $n = 3$ for other conditions). Statistical significance relative to control is indicated when appropriate (ns $p \geq 0.05$, * $p < 0.05$, ** $p \leq 0.01$, *** $p \leq 0.001$, **** $p \leq 0.0001$). Control, cells incubated with FD10 alone; FD10, FITC-dextran 10 kDa; MSNP, propylamine-functionalized mesoporous nanoparticle; DEAE, diethylaminoethyl; Dex-NG, dextran methacrylate (MA)-*co*-TMAEMA nanogels with a degree of substitution (DS) of 3.4; rMFI, relative mean fluorescence intensity.

a relative mean fluorescence intensity (rMFI) of ≈5) compared to MSNPs (≈20% positive cells, ≈1.7 rMFI) (Figure 2b,c). These data suggest marked differences in cell membrane interactions between soluble cationic polymers and cationic nanoparticles. Moreover, these results indicate that membrane destabilizations caused by cationic nanoparticles can indeed be exploited for the

**ADVANCED
SCIENCE NEWS**

www.advancedsciencenews.com

**ADVANCED
MATERIALS**

www.advmat.de

cytosolic delivery of membrane-impermeable macromolecules and that the delivery efficiency can strongly differ between nanoparticle types. This observation is in line with previous reports where both the extent of induced nanoscale membrane deformations as well as their lifetime were found to be highly dependent on the type of material used,[34] which could thus strongly impact cytosolic delivery efficiency. Given their relatively high extent of delivery, dextran nanogels were selected to further explore their delivery potential.

## 3. Scrutinizing Nanogel Properties for Improved Cytosolic Cargo Delivery

To promote the cytosolic delivery efficiency of the dextran nanogels, we investigated the impact of several physicochemical parameters reported to influence polycation-mediated membrane disruption.[35,36,42,45,46] As **Figure 3**a illustrates, cationic dextran nanogels (≈200 nm) are synthesized by copolymerizing methacrylated dextran (dex-MA) with a cationic methacrylate monomer (i.e., [2-(methacryloyloxy)ethyl]-trimethylammonium chloride; TMAEMA) using a mini-emulsion UV polymerization technique.[47] Through the use of dextrans with varying degrees of methacrylate substitution (DS), defined as the amount of methacrylate groups per 100 glucopyranose residues, nanogels with different crosslink densities and network pore sizes can be obtained (Figure 3a).[47–51] To assess the influence of hydrogel crosslink density on the cytosolic delivery efficiency of FD10, we synthesized three nanogel types using methacrylated dextrans with mounting DS values (dex-NG DS 3.4, dex-NG DS 4.7, and dex-NG DS 5.9), while keeping both nanogel size (≈200 nm) and zeta potential (≈+21 mV) constant. The polydispersity index (PDI) of all particles was <0.2 (Table S1, Supporting Information). As demonstrated in Figure 3, all synthesized nanogels enable high cytosolic FD10 delivery in HeLa cells in a dose-dependent manner. Of note, when correlating delivery efficiency with cell viability, dextran nanogels with the highest DS value seem to perform best, with near 100% positive cells while maintaining high cell viability (> 80%) at an optimal nanogel concentration of 150 µg mL⁻¹. On the other hand, the nanogels with intermediate DS 4.7 display both the lowest FD10 delivery and cell viability. Higher crosslink densities not only result in increased stiffness of the hydrogel network, but also correspond with a higher fraction of hydrophobic methacrylate moieties. While particle rigidity is negatively correlated[46] with membrane destabilization, the inverse relation has been described for particle hydrophobicity.[35,42] For example, Liechty et al. recently demonstrated that incorporating hydrophobic moieties into a hydrogel network could significantly alter its cell membrane disruption properties.[52] This discrepancy could explain why no clear linear correlation between the DS value and FD10 delivery efficiency was observed.

For many polycationic materials, cationic charge density has been consistently reported as a major predictor for induced membrane defects.[36,42,46] To investigate the effect of cationic charge, three additional dextran nanogels were synthesized by incorporating different fractions of the cationic methacrylate TMAEMA into the dex-MA DS 5.9 hydrogel network (**Figure 4**a). Stable nanogels could be obtained with a zeta-potential of +10 mV, +16 mV, and +21 mV, while again maintaining a nanogel size of ≈200 nm (Table S1, Supporting Information). In contrast to the DS factor, a clear impact of surface charge on FD10 delivery efficiency was observed, as only nanogels with a sufficiently high cationic charge (i.e., zeta potential of +21 mV) could successfully deliver FD10 into the cytosol of HeLa cells (Figure 4b–d). As the charge density can influence both the number of cationic nanogels adhering to the negatively charged cell membrane[53,54] as well as the interaction strength of individual nanogels with specific cell membrane components, it remains unclear which of these processes is responsible for the observed difference in delivery efficiency. Nonetheless, given the high delivery efficiencies reported for dextran nanogels with a zeta potential of +21 mV and a DS of 5.9, this nanogel formulation was selected to further explore the mechanisms involved in nanogel-mediated membrane disruption.

4. A Crosslinked Hydrogel Network is Required for Cytosolic Macromolecule Delivery

Both cationic nanocarriers used in our initial screen (i.e., MSNPs and dextran nanogels) have been shown to induce membrane perturbations in living cells.[34,35,44] Interestingly, our results suggest that only (spherical) nanoparticles and not linear polymers were able to provoke membrane defects large enough for the passage of FD10 (Figure 2b,c). To further confirm whether an intact hydrogel network was required for dextran nanogel-mediated delivery, we synthesized a degradable cationic dextran nanogel composed of dextran chains substituted with hydroxyethyl methacrylate (dex-HEMA-NG DS 5.2), leading to labile crosslinks with a carbonate ester moiety that hydrolyzes in an aqueous environment.[51,55,56] In contrast, dex-MA-*co*-TMAEMA nanogels (dex-NG DS 5.9) do not contain these degradable crosslinks and retain a stable 3D network over time (Figure S2, Supporting Information).[47,57] As can be seen in **Figure 5**, dex-HEMA-NG (size ≈200 nm, zeta-potential ≈+21 mV, Table S1, Supporting Information) can successfully deliver FD10 into HeLa cells upon co-incubation at subtoxic concentrations (cell viability > 80%, Figure S1, Supporting Information), albeit with significantly lower efficiency relative to the previously optimized dex-NG DS 5.9 nanogel. Remarkably and importantly, degrading the dex-HEMA-NG (24 h incubation at 37 °C) prior to administration to HeLa cells completely abolished cytosolic FD10 delivery, in strong contrast to their stable dex-MA counterpart (dex-NG) exposed to equal experimental conditions. These results confirm the need for an intact 3D network for efficient dextran nanogel-mediated cytosolic FD10 delivery. Hydrolysis of the crosslinks in dex-HEMA-*co*-TMAEMA nanogels will lead to the release of neutral dextran chains and charged linear HEMA-*co*-TMAEMA oligomers, which do not evoke membrane perturbation. These data further corroborate the observed differences in delivery efficiency between linear cationic polymers and cationic nanoparticles (Figure 2). Previous reports have also indicated the importance of polymeric shape towards membrane disruption.[35,36] For example, Hong et al. reported sphere-liked polymeric structures (e.g., PAMAM dendrimers) and branched cationic polymers (e.g., branched PEI) being more effective than linear
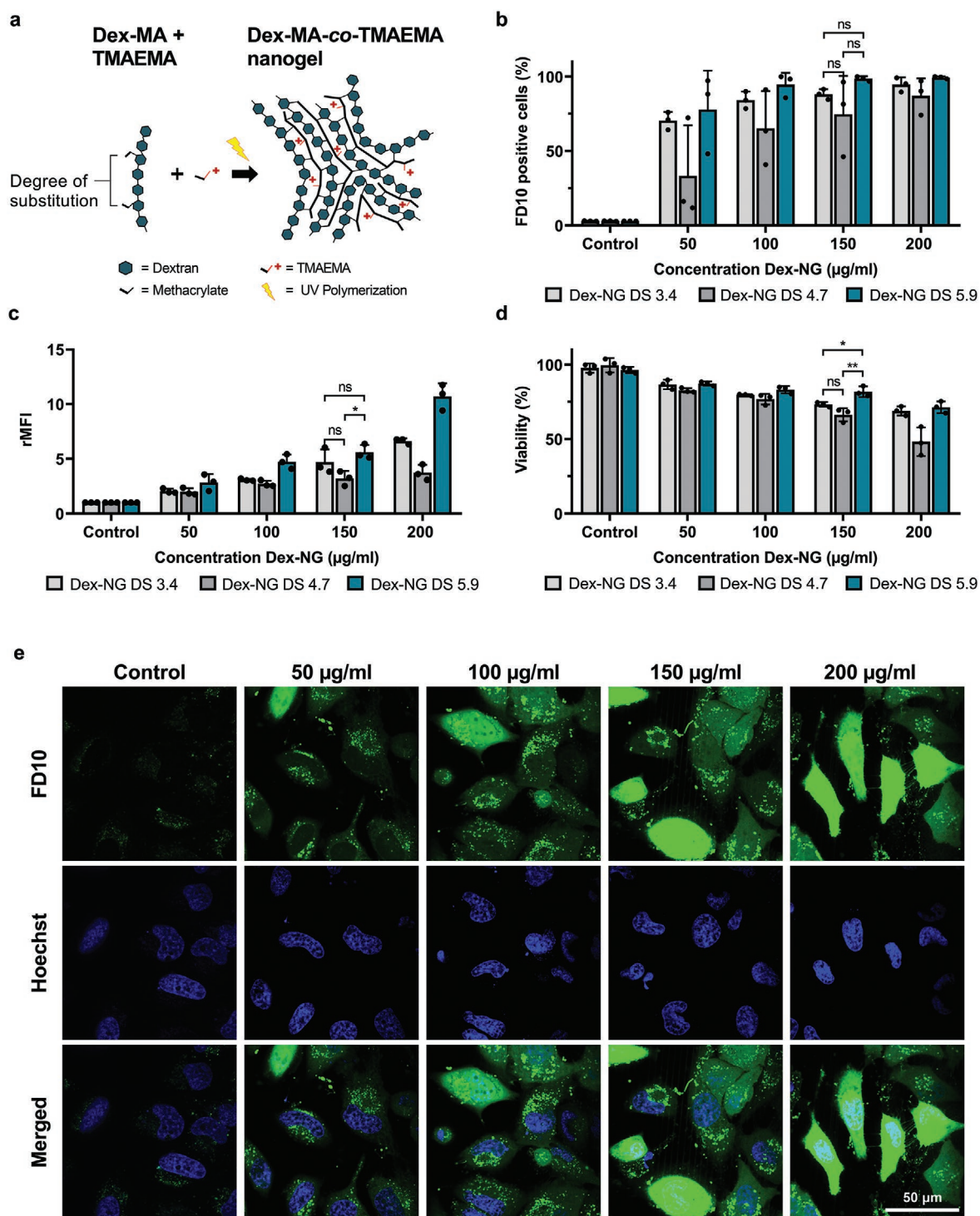
Figure 3. Impact of the methacrylate substitution degree of dextran nanogels on macromolecule delivery in HeLa cells. a) Schematic representation of the synthesis of dex-MA-*co*-TMAEMA nanogel networks and methacrylate degree of substitution (DS). b,c) HeLa cells were incubated for 2 h with dextran nanogels with a substitution degree of 3.4, 4.7, or 5.9 (dex-NG DS 3.4, dex-NG DS 4.7, and dex-NG DS 5.9) in the presence of FITC-labeled dextran 10 kDa (FD10). Quantitative analysis of FD10 delivery in HeLa cells based on nuclear FITC fluorescence intensity, as previously described (>200 cells were imaged and analyzed per condition). d) Cell viability of HeLa cells as measured using an ATP-based viability assay 4 h after dextran nanogel exposure. Data represent mean ± SD of three independent experiments ($n = 3$). Statistical significance is reported where relevant (ns $p \geq 0.05$, * $p < 0.05$, ** $p \leq 0.01$, *** $p \leq 0.001$, **** $p \leq 0.0001$). e) Representative confocal images of FD10 delivery in HeLa cells. Cell nuclei were stained with Hoechst (blue). Green punctae seen in the cell cytoplasm are indicative for FD10 molecules trapped in endosomes. A diffuse cytosolic and nuclear staining corresponds with free cytosolic FD10. Control, cells incubated with FD10 alone; FD10, FITC-dextran 10 kDa; dex-NG, dextran methacrylate (MA)-*co*-TMAEMA nanogels; DS, degree of substitution; TMAEMA, [2-(methacryloyloxy)ethyl]-trimethylammonium chloride; rMFI, relative mean fluorescence intensity.
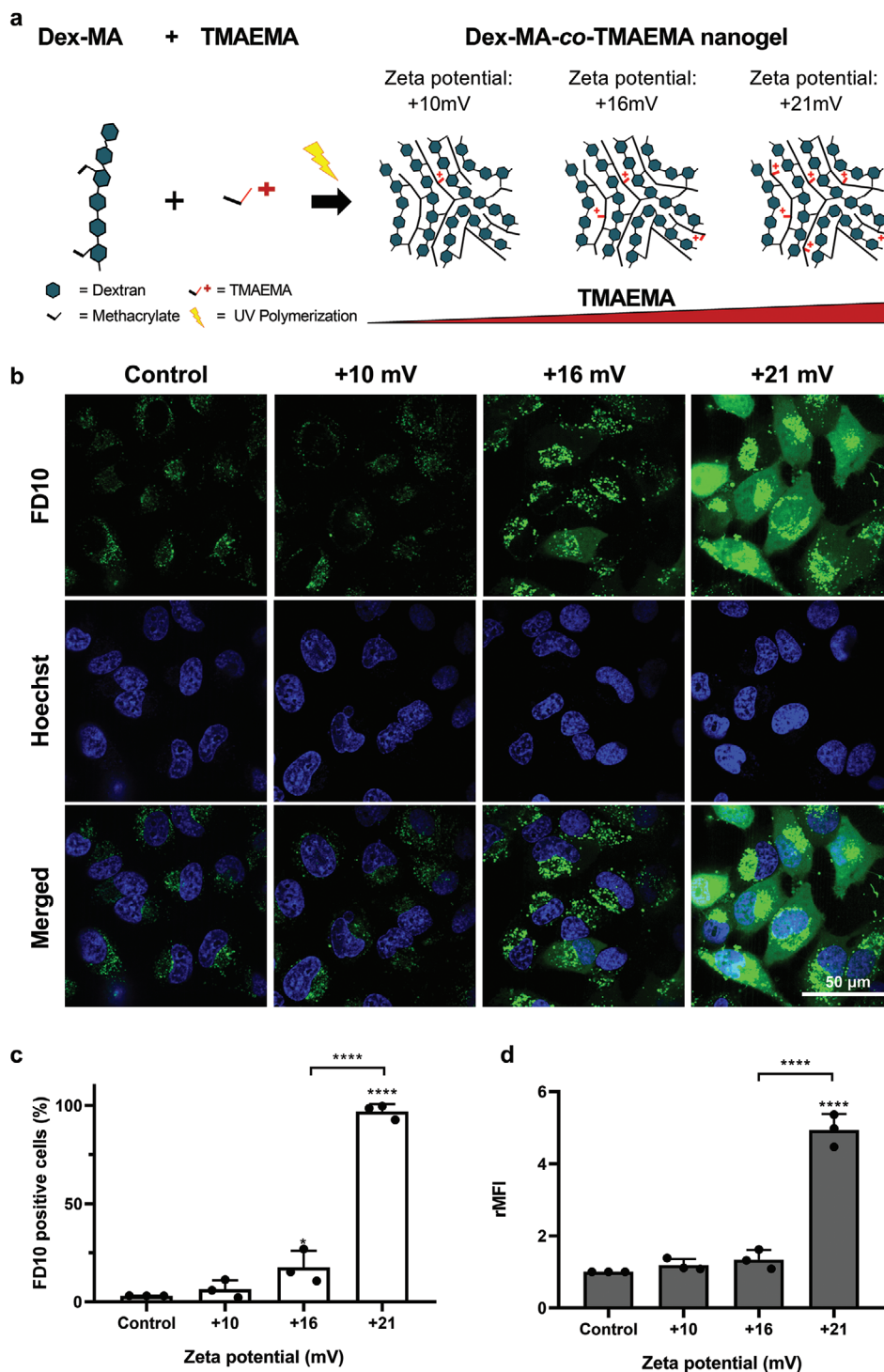
Figure 4. The impact of dextran nanogel cationic charge on macromolecule delivery in HeLa cells. a) Schematic representation of the synthesis of Dex-MA-*co*-TMAEMA nanogels with varying zeta potential by UV polymerizing dex-MA (DS 5.9) with mounting concentrations of the cationic methacrylate TMAEMA. b) HeLa cells were incubated for 2 h with dex-NG DS 5.9 nanogels with a zeta potential of +10 mV, +16 mV, or +21 mV in the presence of FITC-dextran 10 kDa (FD10). Representative confocal images of FD10 delivery in HeLa cells are shown. Cell nuclei were stained with Hoechst (blue). Green punctae seen in the cell cytoplasm are indicative for FD10 molecules trapped in endosomes. A diffuse cytosolic and nuclear staining corresponds with free cytosolic FD10. c,d) Quantitative analysis of FD10 delivery in HeLa cells based on nuclear FITC fluorescence intensity, as previously described (>200 cells were imaged and analyzed per condition). Data represent mean ± SD of three independent experiments ($n = 3$). Statistical significance is reported where relevant (ns $p \geq 0.05$, * $p < 0.05$, ** $p \leq 0.01$, *** $p \leq 0.001$, **** $p \leq 0.0001$). Control, cells incubated with FD10 alone; FD10, FITC-dextran 10 kDa; Dex-NG, dextran methacrylate (MA)-*co*-TMAEMA nanogels; DS, degree of substitution; TMAEMA, [2-(methacryloyloxy) ethyl]-trimethylammonium chloride; rMFI, relative mean fluorescence intensity.

**ADVANCED
SCIENCE NEWS**

www.advancedsciencenews.com

**ADVANCED
MATERIALS**

www.advmat.de
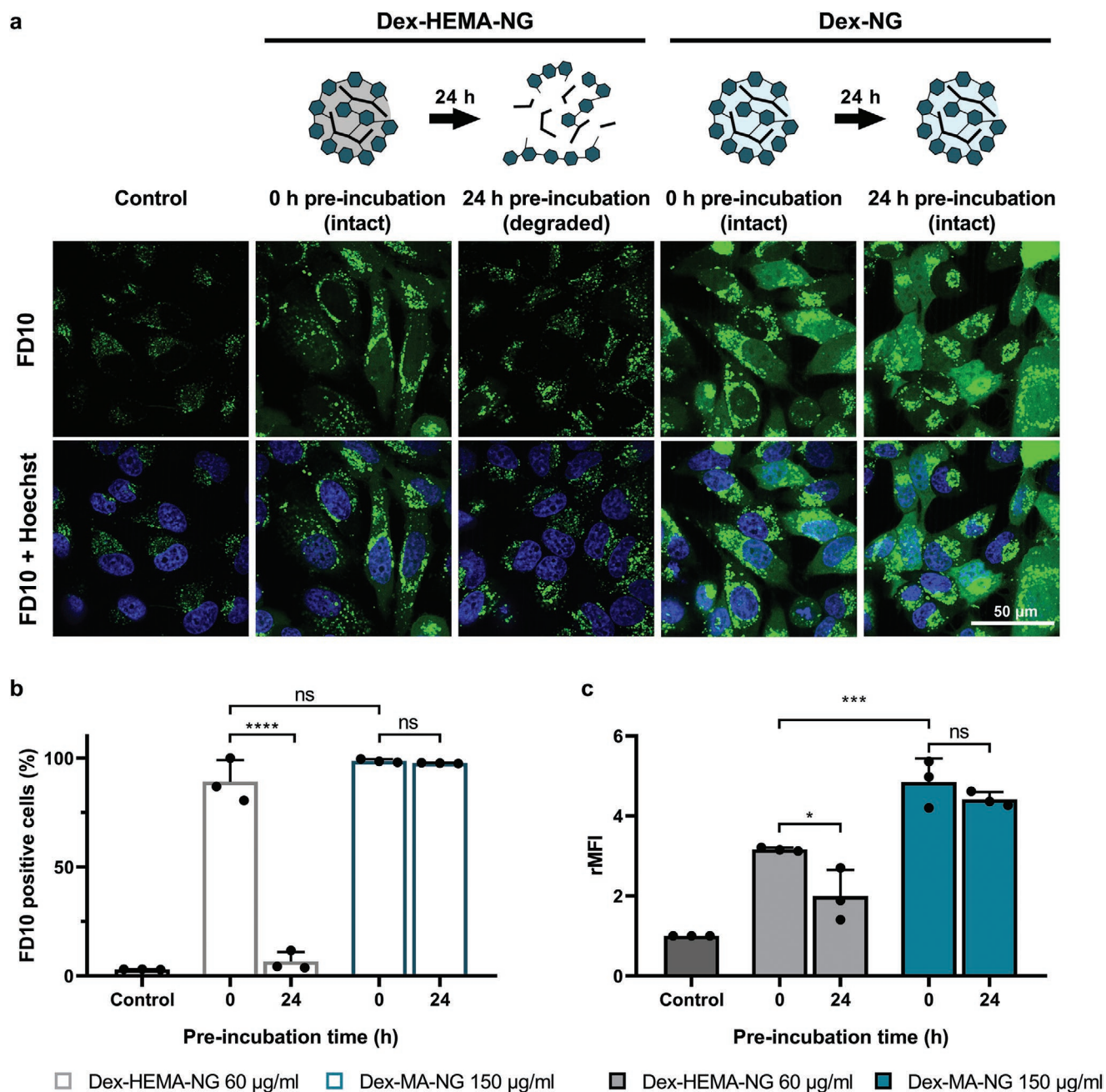
Figure 5. A crosslinked hydrogel network is required for nanogel-mediated macromolecule delivery in HeLa cells. HeLa cells were incubated for 2 h with freshly hydrated dex-HEMA-NG or hydrolyzed dex-HEMA-NG (24 h pre-incubation at 37 °C) in the presence of FD10. Dex-HEMA-NG contain a hydrolysable carbonate ester in their crosslinks rendering them biodegradable in aqueous environment, in contrast to the stably crosslinked dex-NG. a) Representative confocal images of FD10 delivery in HeLa cells. Cell nuclei were stained with Hoechst (blue). Green punctae seen in the cell cytoplasm are indicative for FD10 molecules trapped in endosomes. A diffuse cytosolic and nuclear staining corresponds with free cytosolic FD10. b,c) Quantitative analysis of FD10 delivery in HeLa cells based on nuclear FITC fluorescence intensity, as described previously (>200 cells were imaged and analyzed per condition). Data represent mean ± SD of three independent experiments ($n = 3$). Statistical significance is reported where relevant (ns $p \geq 0.05$, * $p < 0.05$, ** $p \leq 0.01$, *** $p \leq 0.001$, **** $p \leq 0.0001$). Control, cells incubated with FD10 alone; FD10, FITC-dextran 10 kDa; rMFI, relative mean fluorescence intensity; dex-HEMA-NG, dextran-hydroxyethylmethacrylate (HEMA)-*co*-TMAEMA nanogels; dex-NG, dextran-methacrylate (MA)-*co*-TMAEMA nanogels.

polymers at increasing membrane permeability.[36] Importantly, these data additionally suggest that transient membrane disruption with degradable nanogels can be envisioned, in which the membrane destabilizing effect is gradually lost as a function of hydrogel degradation kinetics. Moreover, ex vivo degradation of the nanogels could facilitate their removal from the final product prior to in vivo administration to patients, which is expected to contribute to the overall safety of the approach.

5. Dextran Nanogels Successfully Deliver FITC-Dextran Molecules of Higher Molecular Weight into the Cytosol

Next, we aimed to investigate to which extent the membrane destabilizations created by dex-MA nanogels (dex-NG) can be used to deliver larger molecules by incubating the HeLa cells with the nanogels in the presence of FITC-labeled dextrans with varying molecular weight (i.e., FD 4 kDa, FD 10 kDa, FD 20 kDa, and FD 40 kDa) (**Figure 6**). A clear correlation between the FD size and cytosolic delivery efficiency was seen both for the percentage of positive cells and the measured FITC rMFI in the cell nucleus. A FD molecular weight of 40 kDa (FD40) still resulted in ±70% of positive cells (Figure 6b,c), indicating that the delivery efficiency is only moderately reduced with increasing FD molecular weight. However, the decrease in rMFI as a function of FD molecular weight is more pronounced. This most likely results from a progressively lower fraction of sufficiently large, induced nanoscale defects able to mediate the entry of molecules higher in molecular weight (40 kDa and higher). Given that FD40 has a reported average diameter of 9 nm,[58] these data are still within the range of previously described dimensions of nanoscale membrane pores caused by polycationic materials.[34]

6. Dextran Nanogel-Mediated Cytosolic Macromolecule Delivery is Endocytosis-Independent

Dex-NG DS 5.9 nanogels are known to be taken up by endocytosis.[47] In addition, an increase in endocytic FD10 uptake was seen when co-incubated with cationic nanogels (Figures 2–6). Therefore, it is conceivable that the observed cytosolic FD delivery could occur through nanogel-induced permeabilization of the plasma membrane, the endosomal membrane or both. To investigate the role of endocytic uptake and subsequent endosomal escape in the cytosolic FD10 delivery process, dex-NG nanogels were first loaded with Cy5-labeled RNA to allow their visualization inside cells via confocal fluorescence microscopy (**Figure 7**a). RNA loading was performed at an optimized loading ratio as to not interfere with the dex-NG mediated FD delivery process (Figure S3, Supporting Information). Such a dual labeling approach allows to correlate endocytic uptake, as measured from the endosomal Cy5 signal, with the cytosolic FD delivery efficiency, for which the nuclear rMFI is a proxy.

Endocytic uptake was quantified as the total nanogel fluorescence (Cy5 MFI) for each individual cell (Figure 7b) as well as the total number of nanogel-containing endosomes per cell averaged over the cell area (endosome per 100 μm² cell area) to compensate for differences in cell size (Figure 7c). Using linear regression, no significant correlation could be seen between cytosolic FD delivery and neither total nanogel uptake nor endosome count. In addition, when probing the kinetics of nanogel-induced membrane disruption in HeLa cells, using the membrane-impermeable small molecule nuclear stain propidium iodide (PI), cytosolic delivery was already observed within 5 min (Figure S4, Supporting Information). At 30 min, all cells stained positive for PI after which a linear increase in PI rMFI per cell was observed. Besides demonstrating that this method also enables cytosolic entry of membrane-impermeable small molecules, such fast kinetics of membrane disruption and material influx is in strong contrast with the typically delayed endocytic uptake observed in similarly sized nanoparticles.[59–61] Taken together, these data indicate that the nanogel-mediated cytosolic delivery process is not correlated with endocytic uptake and, therefore, likely primarily occurs at the level of the plasma membrane due to pore formation. As such, we termed this newfound delivery platform HyPore, named after its Hydrogel-enabled nanoPoration effect on cell membranes.

Many theories on how cationic nanocarriers could induce cell membrane disruption have been reported with varying degrees of evidence. Using model cell membranes, Lin et al. described an electroporation-based model in which cationic nanoparticles adhering to negatively charged membrane proteins cause strong local potential differences, driving the formation of transient nanosized holes.[45] Using giant unilamellar vesicles, Li et al. hypothesized that high levels of nanoparticle–membrane binding increases membrane surface tension, possibly causing the formation of transient pores.[44] Lastly, theoretical and computer simulation modelling performed by Ginzburg et al. inferred that the presence of cationic charges in nanoparticles causes a strong attraction of membrane-associated lipid headgroups to the nanoparticle surface, causing the formation of a lipid bilayer around the nanoparticle. When sufficient phospholipids are thus removed from the cell membrane, membrane thinning or ruptures can occur.[42] Furthermore, it has been proposed that polycationic hydrogels can attract anionic lipids into their internal pore structure, leading to microbial membrane disruption.[62] However, at this point, the exact mode of action of the nanogel-mediated plasma membrane poration of mammalian cells remains unresolved and will require additional biological and biophysical experimentation.

7. Dextran Nanogels Efficiently Deliver Macromolecules into Primary Human T Cells

Human T cells are suspension cells that are notoriously hard to transfect with conventional carrier-based transfection techniques, in part due to their limited endocytic capacity, thinner cell membrane and relatively low protein content.[63,64] For these reasons, nucleofection (i.e., an electroporation-based delivery technique) is currently considered the gold standard for the non-viral delivery of macromolecular cargo in these refractory cells. Although we show here that nucleofection can indeed lead to high delivery efficiencies of FD10 in primary human T cells (>95% positive cells, **Figure 8**a), it is also associated with substantial loss of cell viability (≈25% remaining cell viability, Figure 8b). It is important to note that cell viability was assessed via a metabolic assay (CellTiter-Glo) instead of commonly applied live-dead staining for quantification of cell viability via flow cytometry (e.g., with PI or 7-AAD). As the latter does not account for treatment-induced cell lysis or fragmentation, it may lead to an overestimation of cell viability. Having established that dextran nanogel (HyPore)-mediated cytosolic

**ADVANCED
SCIENCE NEWS**

www.advancedsciencenews.com

**ADVANCED
MATERIALS**

www.advmat.de
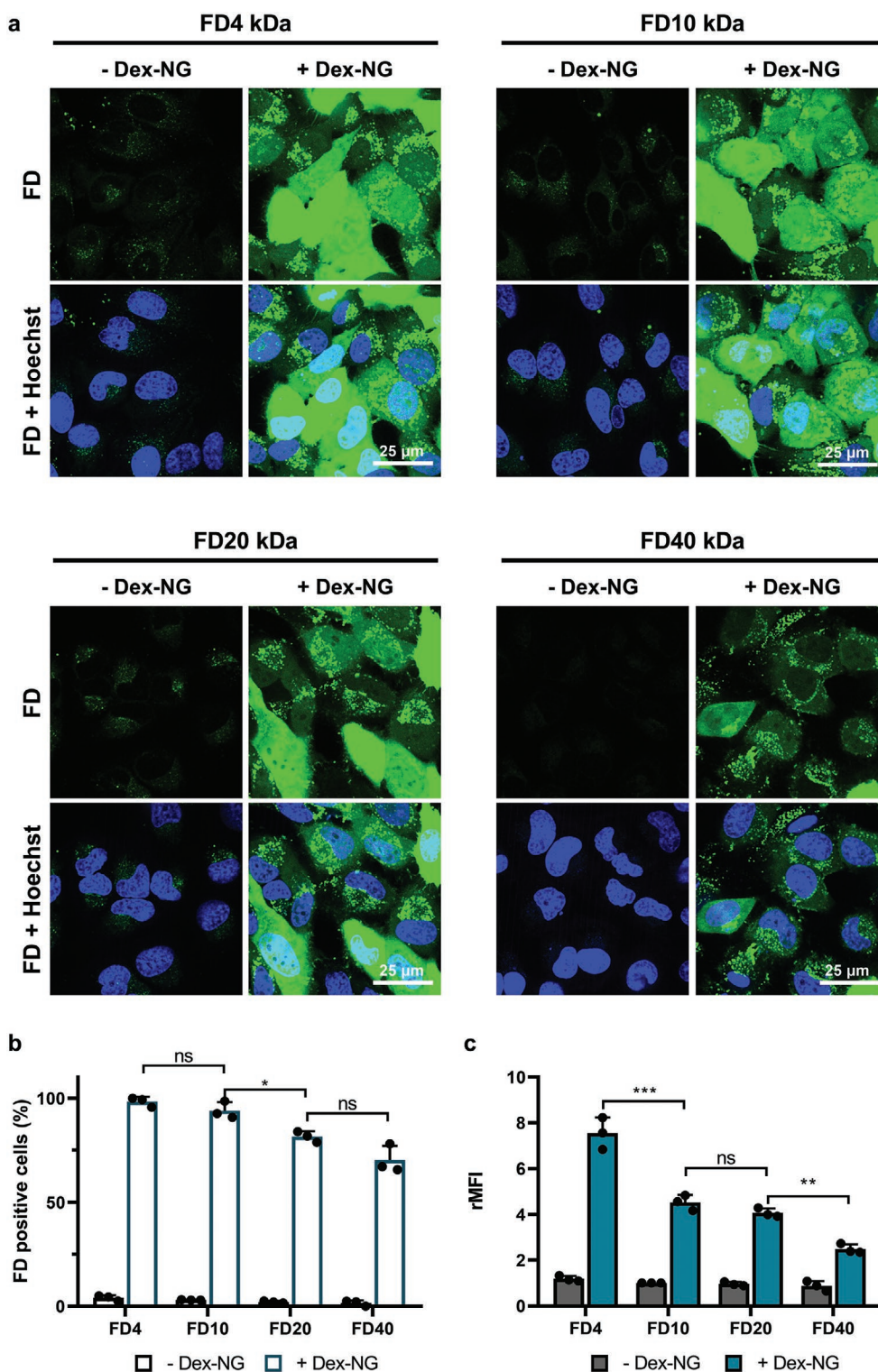
Figure 6. Dextran nanogels can effectively deliver FITC dextrans of up to 40 kDa in HeLa cells. HeLa cells were incubated for 2 h with dex-NG DS 5.9 nanogels in the presence of FITC-dextran with an average size of respectively 4, 10, 20, or 40 kDa (FD4, FD10, FD20, or FD40). a) Representative confocal images of FD4-40 delivery in HeLa cells. Cell nuclei were stained with Hoechst, shown in blue (Hoechst). FD4-40 fluorescence is shown in green (FITC). Green punctae seen in the cell cytoplasm are indicative for FD4-40 molecules trapped in endosomes. A diffuse cytosolic and nuclear staining corresponds with free cytosolic FD4-40. b,c) Quantitative analysis of FD4-40 delivery in HeLa cells based on nuclear FITC fluorescence intensity, as described previously (>200 cells were imaged and analyzed per condition). Data represent mean ± SD of three independent experiments ($n = 3$). Statistical significance is reported where relevant (ns $p \geq 0.05$, * $p < 0.05$, ** $p \leq 0.01$, *** $p \leq 0.001$, **** $p \leq 0.0001$). Control, cells incubated with FD4-40 alone; dex-NG, dextran methacrylate (MA)-*co*-TMAEMA nanogels; rMFI, relative mean fluorescence intensity.
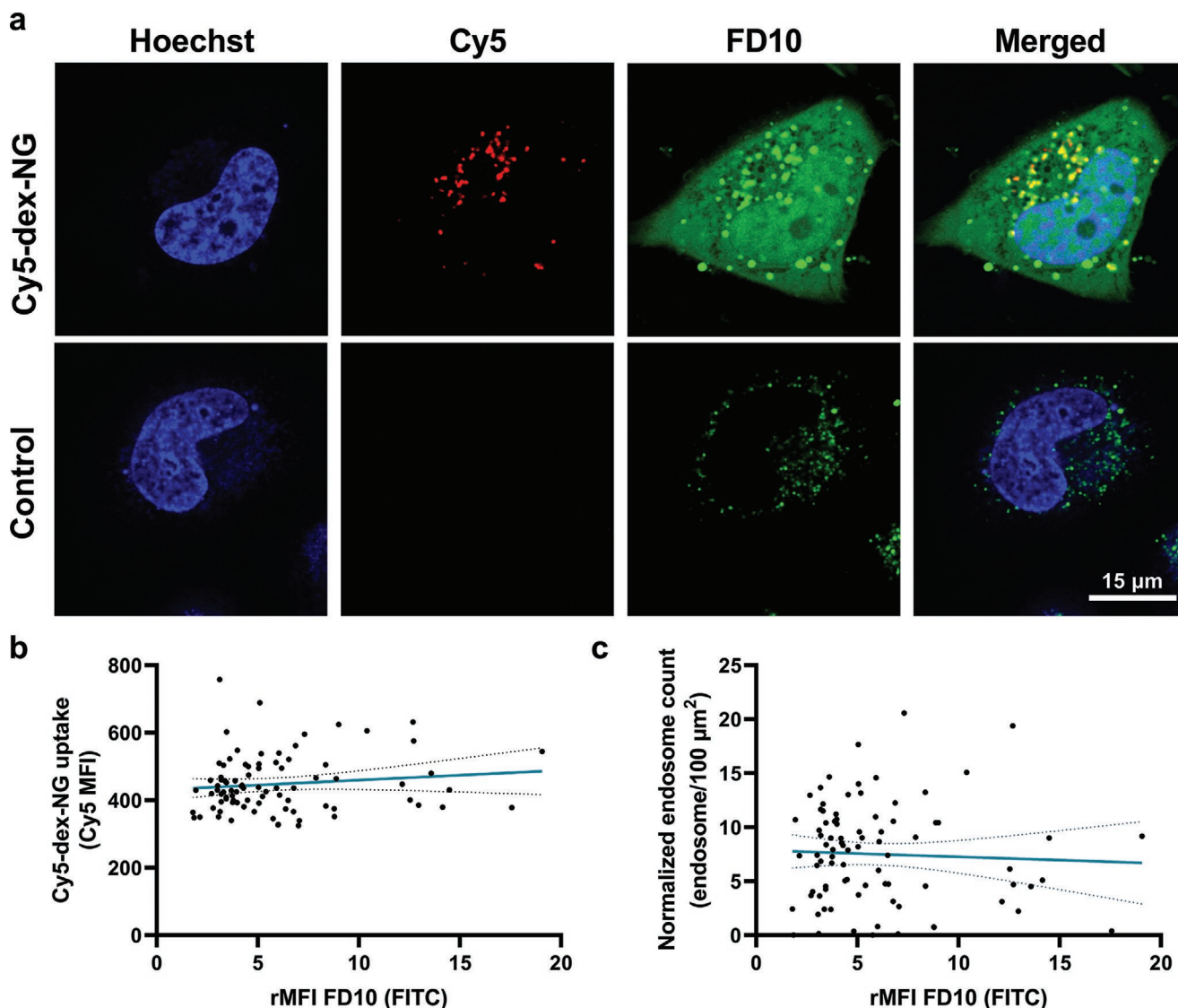
Figure 7. Dextran nanogel-mediated cytosolic FITC dextran delivery is endocytosis-independent. HeLa cells were incubated for 2 h with dex-NG DS 5.9 nanogels, loaded with Cy5-labeled RNA (Cy5-dex-NG), in the presence of FITC-dextran 10 kDa (FD10). a) Representative confocal images of FD10 delivery and Cy5-dex-NG uptake in HeLa cells. Cell nuclei were stained with Hoechst (blue). Red and green punctae are indicative of Cy5-dex-NG and FD10, respectively, trapped in endosomes. A diffuse cytosolic and nuclear FITC staining corresponds with free cytosolic FD10. b) Scatter plots between FD10 delivery (nuclear rMFI FITC) and Cy5-dex-NG uptake were investigated using simple linear regression analysis for 86 cells. The dashed line represents the 95% confidence band of the regression line. The magnitude (between 0 and 1) of the regression coefficient indicates the strength of correlation ($R^2 = 0.015$). A p value below 0.05 indicates that the slope of the curve significantly differs from 0 ($p = 0.26$). c) Correlation between FD10 delivery (rMFI FITC) and total amount of Cy5-dex-NG containing endosomes in individual cells was investigated using simple linear regression analysis (86 cells, $R^2 = 0.002$, $p = 0.67$). Experimental data shown are one representative of three independent experiments with a minimum of 50 cells analyzed per repeat. Control, cells incubated with FD10 alone; rMFI, relative mean fluorescence intensity; dex-NG, dextran methacrylate (MA)-co-TMAEMA nanogels.

delivery was independent of endocytosis, these hydrogel nanoparticles were likewise tested for FD10 delivery in this primary suspension cell type. Optimal delivery was achieved at significantly lower nanogel concentrations compared to adherent HeLa cells (25 μg mL^{-1} versus 150 μg mL^{-1} for HeLa cells), indicating a clear difference in cell membrane-nanoparticle interactions. HyPore effectively delivered FD10 in >50% of primary T cells, while also maintaining >50% cell viability (Figure 8a–c). To compare the efficiency of both nucleofection and HyPore-based FD delivery in more detail, we calculated the delivery

yield and rMFI of both techniques. The yield is expressed as the percentage of viable cells loaded with cytosolic FD10 and is the product of both the cell viability and the percentage of FD-positive cells. HyPore-mediated delivery realized a comparable delivery yield (28%) relative to nucleofection (22%) (Figure 8d). Importantly however, the amount of FD10 delivered per cell was about 2.5-fold higher for the HyPore protocol, with an rMFI of 20.9 compared to 8.6 for nucleofection. This marked difference could be explained by the longer incubation time offered by the HyPore delivery platform during which cargo can diffuse into

ADVANCED
SCIENCE NEWS

www.advancedsciencenews.com

ADVANCED
MATERIALS

www.advmat.de
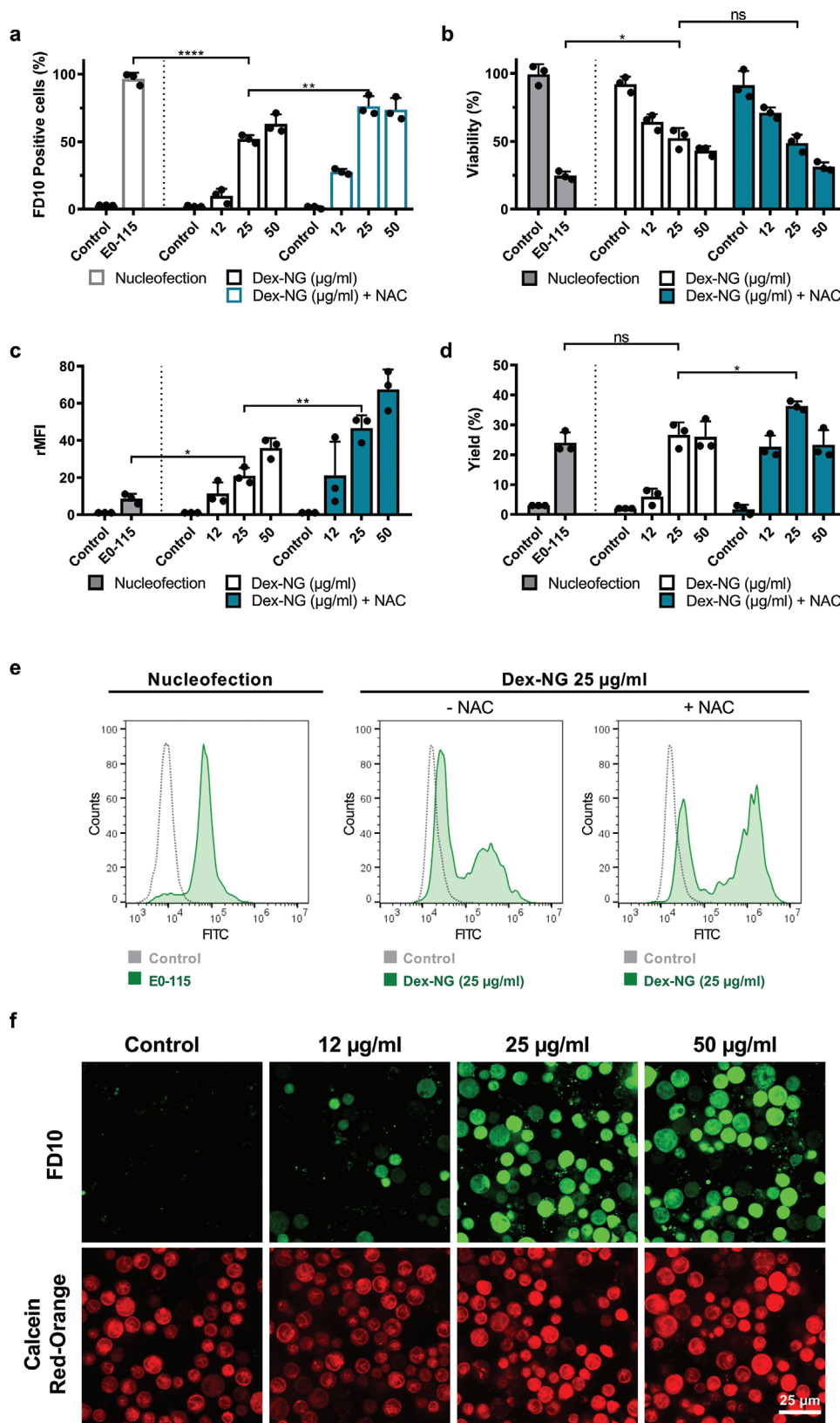
Figure 8. Dextran nanogel-mediated FD10 delivery outperforms nucleofection in primary human T cells. Human T cells were isolated from peripheral blood mononuclear cells and expanded for several weeks. Next, cells were resuspended in Opti-MEM or Opti-MEM supplemented with 10×10^{-3} M N-acetylcysteine (NAC) and incubated for 1 h with dextran nanogels in the presence of FITC-dextran 10 kDa (FD10). a) Quantitative analysis of FD10

**ADVANCED
SCIENCE NEWS**

www.advancedsciencenews.com

**ADVANCED
MATERIALS**

www.advmat.de

the porated cell. This is in contrast with nucleofection, where generated pores remain open for only a short time (seconds to minutes), thus limiting diffusion-mediated influx.[65] Furthermore, as FD10 is a neutral macromolecule, no electrophoretic influx is present during electroporation.[66] This observed delivery advantage is particularly relevant for T cells given their high cell division rate upon activation. As T cells divide, the cytosolic cargo is diluted over future generations of daughter cells, which can be a limiting factor in certain therapeutic applications as the intracellular titers fall below the minimal effective concentration.[67,68]

Cellular toxicity induced by polycationic materials, including cationic dextran nanogels, is partially mediated through the formation of reactive oxygen species (ROS), which can be alleviated by the ROS scavenger N-acetylcysteine (NAC).[38] In addition, NAC is FDA-approved for various medical uses (e.g., paracetamol overdose, chronic obstructive pulmonary disease)[69] and has recently shown to markedly increase the efficacy of adoptive T cell therapy by improving both T cell mediated tumor control as well as T cell persistence and survival in mice.[70,71] As such, to further optimize the yield of nanogel-mediated macromolecule delivery in human T cells, NAC was added to the cell medium during nanogel incubation. Unexpectedly, the presence of NAC could not improve T cell viability in our hands (Figure 8b). In contrast, NAC markedly improved the FD10 delivery efficiency, with increased numbers of FD10-positive cells (>70%) and rMFI values (46.7), further outperforming nucleofection (Figure 8a–f, Figure S5, Supporting Information). The beneficial effect of NAC co-treatment on cytosolic delivery could not be replicated with β-mercaptoethanol, another ROS scavenger commonly used in T cell cultures (Figure S6, Supporting Information). Interestingly, when HeLa cells were treated with a combination of NAC and HyPore, a decrease in FD delivery was observed, suggesting that the delivery-promoting effect of NAC is cell type-dependent.

Furthermore, T cell membrane integrity was shown to be quickly restored after nanogel treatment, as human T cells appear impermeable for TO-PRO-3 iodide after a single wash step following HyPore exposure (Figure S7, Supporting Information). TO-PRO-3 iodide is a cell-impermeable membrane exclusion dye that can only enter cells of which membrane integrity is compromised. These results were also seen in HeLa cells (Figure S7, Supporting Information) and confirm the fast recovery times ($\approx 10^{-1}$s) of cationic nanocarrier-induced membrane destabilizations reported in the literature. Finally, in addition to HeLa cells and primary human T cells, dextran nanogels were also able to efficiently deliver FD10 to H1299 non-small cell lung cancer cells (data not shown), RAW264.7 cells (murine macrophage cell line), and primary bovine corneal epithelial cells (PBCEC) (Figures S8 and S9, Supporting Information, respectively). As such, the HyPore delivery platform demonstrates it can be used to deliver cargo to different cell lines as well as hard-to-transfect primary cells.

8. Dextran Nanogels Allow Intracellular Delivery of Functional Membrane-Impermeable Cargo

Having established that the HyPore protocol can deliver FDs into a variety of cell types, we next sought to probe the delivery of membrane-impermeable cargo with an intracellular functionality. For instance, intracellular delivery of proteins is of high interest to investigate cellular pathways or to manipulate cells for therapeutic applications. Unfortunately, the development of protein biologics against intracellular targets is hampered by their inability to spontaneously cross cellular membranes. Nanobodies are relatively small single variable-domain antibodies, ≈ 15 kDa in size, derived from heavy chain only antibodies typically found in the sera of Camelids.[72] Nanobodies encompass many favorable characteristics compared to conventional full length antibodies, including their small size as well as improved stability and affinity. These specific features rationalize a myriad of biomedical applications, not only as research tools but also as diagnostic and therapeutic agents, for example, for intracellular applications. Nevertheless, such applications will depend on crossing the cell membrane, hence requiring efficient intracellular delivery approaches. To demonstrate cytosolic nanobody delivery with our HyPore delivery platform, a histone-binding nanobody (Histone-Label, HL), conjugated to the fluorescent dye ATTO488, was used. Cytosolic delivery of HL leads to direct staining of chromosomes and nuclei in cell labeling experiments. As demonstrated in **Figure 9**a–c, HyPore-mediated delivery of this fluorescently-labeled nanobody in HeLa cells is remarkably efficient, with over 95% of the cell nuclei successfully stained with a rMFI of 10.8.

As another example, we aimed to demonstrate functional cytosolic delivery of enzymes. Granzyme A is a serine protease present in cytotoxic granules of cytotoxic T lymphocytes and natural killer cells. Such cells co-deliver granzymes with perforin, a membranolytic protein that forms pores in endosomal membranes and thus enables cytosolic granzyme delivery in target cells. However, in absence of perforin, granzymes are not able to reach the cytosol. Its delivery to target cells such as tumor cells or viral-infected cells activates a specific caspase-independent cell death pathway. Co-incubation of HeLa cells with HyPore and granzyme A resulted in highly efficient

delivery efficiency using flow cytometry. Cells were stained with a membrane exclusion dye (TO-PRO-3 iodide) staining dead cells. TO-PRO-3 iodide negative cells were gated for delivery efficiency analysis. b) Analysis of cell viability, 4 h after treatment, using an ATP-based viability assay (CellTiter-Glo). c,d) Quantitative analysis of FD10 delivery efficiency using flow cytometry on TO-PRO-3 iodide negative cells. The yield is determined as percentage living cells (based on CellTiter-Glo assay), multiplied by the percentage of FD10-positive cells. Data shown as mean ± SD of three independent experiments ($n = 3$). Statistical significance is reported where relevant (ns $p \geq 0.05$, * $p < 0.05$, ** $p \leq 0.01$, *** $p \leq 0.001$, **** $p \leq 0.0001$). Control, cells incubated with FD10 alone; dex-NG, dextran methacrylate (MA)-*co*-TMAEMA nanogels; rMFI, relative mean fluorescence intensity. e) Flow cytometry histograms displaying FD10 delivery efficiency upon nucleofection or treatment with 25 µg mL^{-1} of dextran nanogels in the presence or absence of 10×10^{-3} M NAC. f) Representative confocal images of FD10 delivery in human T cells following NAC and dex-NG co-treatment. After treatment, cells were incubated for 10 min with Calcein Red-Orange AM, a cell permeable dye used to determine cell viability. Viable cells are shown in red. A diffuse cytosolic and nuclear FITC staining corresponds with free cytosolic FD10.

Figure 9. HyPore-mediated delivery of functional cargo. a–c) HeLa cells were incubated for 2 h with HyPore in the presence of Histone-Label ATTO488 (nanobody), after which the cells were washed and the nuclei stained with Hoechst (blue). a) Representative confocal images show Hoechst staining (blue) and Histone-Label delivery (green) in HeLa cells. b,c) Quantitative analysis of Histone-label delivery in HeLa cells based on nuclear ATTO488 fluorescence intensity. Data represent mean ± SD of three independent experiments ($n = 3$). Control, incubated with Histone-label alone; HL, Histone-Label ATTO488. d,e) HeLa reporter cells containing the reporter plasmid, pLV-CMV-LoxP-DsRed-LoxP-eGFP, were incubated for 2 h with HyPore in the presence of Cre recombinase. Upon successful delivery of active Cre recombinase, the DsRed gene is floxed and the eGFP gene is expressed resulting in green fluorescent signal. d) Representative confocal images show DsRed expression (magenta) and eGFP expression in HeLa cells. e) Quantitative analysis of functional Cre recombinase delivery in HeLa reporter cells, analyzed using flow cytometry. Both nucleofection and PULSin (complexed with Cre recombinase) treatment were performed according to the manufacturers' instructions. Data represent mean ± SD of three independent experiments ($n = 3$). Control, incubated with Cre recombinase alone; Cre, Cre recombinase enzyme. f–h) HyPore-mediated delivery of gadobutrol in human T cells for magnetic resonance imaging (MRI). f) Chemical structure of gadobutrol, a non-ionic macrocyclic gadolinium-based MRI contrast agent. g,h) Human T cells were incubated for 1 h in Opti-MEM containing HyPore and gadobutrol (Gd-DO3A-butrol). Gadobutrol is an MRI contrast agent that provides a strong T_1 brightening signal. As a positive control, gadobutrol was delivered in human T cells using nucleofection. g) T_1-weighted image of human T cells loaded with gadobutrol using HyPore (with or without N-acetylcysteine (NAC)) or nucleofection and their respective non-treated controls. A strong T_1-weighted signal enhancement can be seen in both HyPore- and nucleofection-treated cells. h) Normalized relaxation values ($R_1 = T_1^{-1}$) are shown. Data represent mean ± SD of at least two independent experiments ($n \geq 2$). Statistical significance is reported where relevant (ns $p \geq 0.05$, * $p < 0.05$, ** $p \leq 0.01$, *** $p \leq 0.001$, **** $p \leq 0.0001$). Gd, gadolinium; HyPore, Hydrogel-enabled nanoPoration via dextran methacrylate (MA)-*co*-TMAEMA nanogels DS 5.9; NTC, non-treated condition; Control, incubated with gadobutrol alone.

cell killing (Figure S10, Supporting Information). Successful enzyme delivery was further confirmed using confocal microscopy, visualizing the externalization of phosphatidylserine with labeled Annexin V, typical for granzyme A-mediated apoptotic cell death (Figure S10a, Supporting Information).

To further demonstrate that HyPore can deliver functional proteins inside cells, we assessed the intracellular delivery of the enzyme Cre recombinase. Cre recombinase is a tyrosine recombinase enzyme derived from the P1 bacteriophage with a size of 38 kDa. Cre binds to a 34 bp long sequence denoted as loxP (locus of crossing (x) over of P1) where it catalyzes a recombination reaction. Its high specificity and efficiency, even when facing complex eukaryotic genomes, explains why even today Cre recombinase remains an important tool for precise and rapid genome editing.[73] Here, we inserted the Cre reporter plasmid pLV-CMV-LoxP-DsRed-LoxP-eGFP in HeLa cells, causing a shift from red (DsRed) to green fluorescence (eGFP) after successful Cre-mediated recombination. Co-incubation of HeLa reporter cells with dextran nanogels and Cre recombinase resulted in 23% of eGFP-expressing HeLa cells (eGFP+) (Figure 9d,e), compared to only 11% eGFP+ cells with PULSin, a commercial delivery reagent for non-invasive protein delivery. As a positive control, nucleofection-mediated delivery resulted in 38% recombination efficiency in these adherent cells. Nonetheless, the ease of use, no requirement for cell detachment or specialized instrumentation, as well as low material cost offer considerable advantages over nucleofection for protein delivery.

Following the high delivery efficiency reported for the HyPore protocol in primary T cells, outperforming nucleofection (Figure 8), we additionally explored the delivery of the small molecular MRI contrast agent gadobutrol (Gd-DO3A-butrol), a neutral gadolinium complex (Figure 9f) that enhances T_1 relaxation (positive contrast) and which can be used for in vivo cell tracking in adoptive cell therapies.[74] As such, the persistence and tissue distribution of adoptively transferred cells can be determined, which is critical to evaluate their immunoregulatory effects in vivo.[67,75] Nonetheless, the cytosolic delivery of gadobutrol into cells is required as high endosomal gadolinium concentrations following pinocytic uptake have been linked with the quenching of relaxivity.[76,77] Here, we evaluated the use of HyPore for the cytosolic delivery of the clinically approved gadobutrol into primary human T cells. Nucleofection was selected as a positive control, for which enhanced T_1-weighted signals in mammalian cells have been reported upon direct cytosolic gadobutrol delivery.[76] Based on the T_1-weighted images (Figure 9g) and the calculated relaxation rates (Figure 9h), significantly higher signal intensities of HyPore-treated human T cells could be seen compared to cells treated with gadobutrol alone, even at relatively low cell numbers (400k). Furthermore, NAC and HyPore co-treatment further improved the observed T_1-weighted signals, resulting in significantly higher contrast compared to nucleofection-mediated gadobutrol delivery (Figure 9g,h).

9. Conclusion

We have reported on the repurposing of cationic hydrogel nanoparticles for transient plasma membrane poration and direct cytosolic delivery of membrane-impermeable cargo. This novel approach, which we dubbed the HyPore protocol, merges beneficial aspects of both membrane disruption- and (non-viral) carrier-mediated intracellular delivery techniques. It enables cytosolic delivery of cargo with diverging physicochemical properties in a variety of cell types, including hard-to-transfect human primary T cells, without the need for an external physical trigger. Importantly, cytosolic delivery neither requires cargo encapsulation/complexation nor endocytic uptake, thus bypassing the need for endosomal escape and cargo release. Furthermore, these features render HyPore a suitable method for cytosolic delivery of neutral and cationic (macromolecular) compounds, for which state-of-the-art intracellular delivery reagents are not readily available. Finally, HyPore employs relatively simple but flexible materials, which are amenable for upscaling while maintaining low production cost. Although HyPore might not be preferred for direct in vivo use, we propose this approach as a highly versatile and cost-effective technique for high-throughput cytosolic cargo delivery for ex vivo manipulation of cells.

10. Experimental Section

Materials: FITC-labeled dextrans (4, 10, 20, and 40 kDa), N-acetylcysteine (NAC), dispase II, dextran sulfate sodium salt (10 kDa), DEAE-dextran (20 kDa), propylamine-functionalized mesoporous silica nanoparticles (MSNPs) and sorbitol-supplemented hormonal epithelial medium (SHEM) were obtained from Sigma-Aldrich (Overijse, Belgium). Hoechst 33342 and CellMask Deep Red Plasma Membrane Stain were purchased from Molecular Probes (Belgium). CellTiter-Glo was obtained from Promega (Leiden, Netherlands). TO-PRO-3 iodide, penicillin, Annexin V (FITC conjugate), Dulbecco's modified Eagle medium (DMEM)/F12, DMEM, Iscove's modified Dulbecco's medium (IMDM), Roswell Park Memorial Institute (RPMI) medium, phosphate buffered saline (PBS), CO_2-independent medium and 1% agar were acquired from Invitrogen (Merelbeke, Belgium). Histone-Label ATTO488 was obtained from Chromotek (Planegg-Martinsried, Germany). Cre recombinase was purchased from New England Biolabs (Mississauga, Canada). Human recombinant granzyme A was purchased from Biolegend (San Diego, USA). Gadavist (gadobutrol) was acquired from Bayer (Leverkusen, Germany). Puromycin was purchased from Gibco (Camarillo, USA). Lymphoprep was purchased from Alere Technologies AS (Oslo, Norway). Immunocult Human CD3/CD28 T cell Activator was from Stemcell Technologies (Vancouver, Canada). Fetal bovine serum (FBS) was purchased from Hyclone (GE Healthcare, Machelen, Belgium). Bovogen (Melbourne, Australia) provided the fetal calf serum (FCS). CELLview culture dishes were purchased from Greiner Bio-One GmbH (Vilvoorde, Belgium). Phytohemagglutinin was purchased from Remel Europe (KENT, UK). IL-2 was purchased from Roche Diagnostics (Mannheim, Germany). PULSin and JetPEI were obtained from Polyplus Transfection (Strasbourg, France). Fluorescent negative control siRNA, labeled with a Cy5 dye at the 5′ end of the (sense) strand (abbreviated Cy5-RNA), was provided by Eurogentec (Seraing, Belgium).

Nanoparticle Synthesis, Preparation, and Characterization: Dextran methacrylate (MA)-*co*-TMAEMA nanogels (dex-NG) and dextran hydroxyethyl methacrylate (HEMA)-*co*-TMAEMA nanogels (dex-HEMA-NG) were synthesized by photopolymerizing respectively dextran methacrylate (dex-MA) or dextran hydroxyethyl methacrylate (dex-HEMA), with the indicated substitution degrees, with the cationic methacrylate monomer [2-(methacryloyloxy)ethyl]-trimethylammonium chloride (TMAEMA), using an inverse emulsion method as previously described.[47] The degree of methacrylate substitution (DS) is defined as the amount of methacrylate groups per 100 glucopyranose residues. By selecting dex-MA with different substitution degrees, nanogels

with different crosslink densities and network pore sizes can be synthesized. Following their synthesis, the nanogels were lyophilized and stored dessicated. To obtain nanogels for in vitro experiments, a weighted amount of lyophilized nanogels was dispersed in RNase free water followed by sonication (3 × 5 s amplitude 10%) using a Branson Digital Sonifer (Danbury, USA). MSNPs were likewise dispersed in RNase free water before experimental use and sonicated (3 × 2 min, amplitude 15%, 10 s on/10 s off). Zeta-potential and hydrodynamic diameter of nanogels and MSNPs were acquired in 4-(2-hydroxyethyl)-1-piperazineethanesulfonic acid (HEPES) buffer (20 × 10^{-3} M, pH 7.4) using a Zetasizer Nano ZS (Malvern), equipped with Dispersion Technology Software.

Cell lines, Primary Cells, and Cell Culture Conditions: HeLa cells were obtained from American Type Culture Collection (ATCC, Manassas, USA) and cultured in DMEM/F12 supplemented with heat-inactivated FBS (10%), L-glutamine (2 mg mL^{-1}) and penicillin/streptomycin (100 U mL^{-1}). HeLa cells containing the Cre reporter construct pLV-CMV-LoxP-DsRed-LoxP-eGFP-IRES-Puro (HeLa reporter cells) were kindly provided by Dr. O. G. de Jong and Dr. P. Vader (University Medical Center Utrecht).[78] These cells were cultured in DMEM supplemented with heat-inactivated FBS (10%), L-glutamine (2 mg mL^{-1}), penicillin/streptomycin (100 U mL^{-1}), and puromycin (2 μg mL^{-1}).

Buffy coats were obtained with informed consent from healthy donors and used following the guidelines of the Medical Committee of the Ghent University Hospital (Belgium, CG20171208A). Peripheral blood mononuclear cells (PBMCs) were isolated from buffy coats via density centrifugation using Lymphoprep. Next, PBMCs were stimulated with Immunocult Human CD3/CD28 T cell Activator and cultured in IMDM supplemented with FCS (10%), penicillin (100 U mL^{-1}), streptomycin (100 μg mL^{-1}), glutamine (2 × 10^{-3} M) and IL-2 (5 ng mL^{-1}) for 7 days. Subsequently, the PBMCs were harvested and maintained in complete IMDM supplemented with IL-2 (5 ng mL^{-1}). When required, T cells were restimulated using a PBMCs and JY feeder cell mixture and phytohemagglutinin (1 μg mL^{-1}). Feeder cells were irradiated using the Small Animal Radiation Research Platform (Xstrahl, Surrey, UK) at respectively 40 Gy and 50 Gy before use. Resting CD3$^+$ cells (referred to as human T cells) were harvested 14 days after stimulation and used for experiments as further indicated.

Freshly excised bovine eyes were collected at a local slaughterhouse (Flanders Meat Group, Zele, Belgium) in cold CO$_2$-independent medium. Within 30 min following collection, excess tissue was removed and the eyes were disinfected by dipping into an ethanol solution (5%). A trephine blade was used to collect 10 mm diameter corneal buttons. The corneal buttons were rinsed with DMEM containing antibiotics and divided in 4 equal parts using a scalpel, rinsed again with DMEM and placed in a Dispase II (15 mg mL^{-1}), SHEM (100 × 10^{-3} M) solution at 37 °C for 10 min. Hereafter, the tissues were rinsed with PBS and placed in a fresh Dispase II-containing medium and kept at 4 °C overnight. The following day the epithelial layer was separated from the corneal stroma using a blunt stainless-steel spatula. To obtain a single cell solution, the epithelial cells were placed in 1 mL of preheated (37 °C) trypsin (0.25%), EDTA (1 × 10^{-3} M) and incubated for 5 min at 37 °C. To neutralize the trypsin, cell medium containing FBS was added after incubation. The obtained primary bovine corneal epithelial cells (PBCEC) were collected via centrifugation (2 min, 1000 rpm) and resuspended in fresh SHEM medium.

Cationic Nanocarrier-Induced Cytosolic Cargo Delivery in Adherent Cells: HeLa cells, PBCEC, and RAW 264.7 cells were seeded respectively at 5 × 10^4, 6.25 × 10^4 and 10 × 10^4 cells per compartment in a 4 compartment, 35 mm diameter glass bottom CELLview culture dish (Greiner Bio-One GmbH, Vilvoorde, Belgium). After 24 h, cells were washed twice using PBS. Next, cells were incubated in Opti-MEM containing the indicated nanomaterial and either FITC-dextran, Histone-Label ATTO488, Cre recombinase or granzyme A at the specified concentrations. Incubations were performed for 2 h at 37 °C in a humidified atmosphere containing CO$_2$ (5%) unless specified otherwise. Next, nanocarriers and excess proteins were washed away using PBS. Cell nuclei were stained in cell culture medium containing Hoechst 33342 (20 μg mL^{-1}) for 15 min.

Finally, the staining solution was removed and fresh cell culture medium was added. Cells were kept at 37 °C in a humidified atmosphere with CO$_2$ (5%) until confocal imaging.

Quantification of FITC-Dextran and Histone-Label ATTO488 Delivery via Confocal Microscopy: Hoechst-stained cells were imaged using a spinning disk confocal microscope, equipped with a Yokogawa CSU-X confocal spinning disk device (Andor, Belfast, UK), a MLC 400 B laser box (Agilent technologies, California, USA) and an iXon ultra EMCCD camera (Andor, Belfast, UK). A Plan Apo VC (60× 1.4 NA) oil immersion objective lens (Nikon, Japan) was used for imaging adherent cell types while human T cells were imaged using a Plan Apo VC (60× 1.2 NA) water immersion lens (Nikon, Japan). NIS Elements software (Nikon, Japan) was applied for imaging. Hoechst 33342 staining and FITC-dextran or Histone-Label ATTO488 were excited sequentially with delay (0.2 s) using a 405 nm (Hoechst 33342) and 488 nm (FITC-dextran or Histone Label ATTO488) laser line. ImageJ (FIJI, Version 1.8.0) software was used to analyze cellular delivery. Nuclei were detected in the blue channel using thresholding, excluding nuclei at the image border. The same threshold settings were maintained for every image. The indicated nuclear region of interest (ROI) was then applied to the green channel to determine the nuclear green fluorescence. A minimum of 200 cells was analyzed per condition unless specified otherwise. These intensity values were plotted as frequency distributions (histograms) and used to determine the percentage of positive cells containing FITC-dextran or Histone-Label ATTO488. The relative MFI was determined as the average mean gray values measured in the green channel (as previously described) divided by the average mean gray value measured in the negative control (i.e., cargo only).

Quantification of Cell Viability: The toxicity of cationic nanomaterials on HeLa cells, PBCEC (2 × 10^4 cells per well) and human T cells (1 × 10^6 cells per well) was measured using a CellTiter-Glo luminescent viability assay (Promega, Belgium) according to the manufacturer's instructions. Cells were seeded 24 h before treatment in a 96-well plate and treated as previously described, incubating them for 2 h (1 h for human T cells) in the presence of a cationic nanomaterial and a cargo molecule. Next, cells were washed and new cell culture medium was added. After 4 h, medium was renewed and an equal volume of CellTiter-Glo reagent was added. Samples were shaken on a shaker plate for 10 min at 100 rpm. Solution (100 μL) was taken from each sample and transferred to an opaque 96-well plate (Greiner Bio-One GmbH, Vilvoorde, Belgium). Sample luminescence was measured using a microplate reader (GloMax).

Correlating Endosomal Uptake with Cytosolic Delivery in HeLa Cells: HeLa cells were seeded at 5 × 10^4 cells per compartment in a 4 compartment, 35 mm diameter glass bottom CELLview culture dish. After 24 h, the cells were washed twice with PBS. Cationic dextran nanogels were fluorescently labeled by mixing them for 15 min with Cy5-RNA to allow electrostatic complexation. Next, HeLa cells were incubated for 2 h in Opti-MEM containing Cy5-RNA loaded dextran nanogels (Cy5-dex-NG) and FITC-dextran 10 kDa (FD10, 2 mg mL^{-1}). Excess Cy5-dex-NG and FD10 were washed away using PBS, followed by a short washing step with dextran sulfate sodium salt (1 mg mL^{-1}, 10 kDa, Sigma-Aldrich) in PBS. Finally, cells were washed using PBS and incubated in cell culture medium containing Hoechst 33342 (20 μg mL^{-1}). Staining solution was removed and fresh cell culture medium was added. Hoechst-stained HeLa cells were imaged using a spinning disk confocal microscope. NIS Elements software (Nikon, Japan) was applied for imaging. Hoechst 33342 staining and FD10 were excited using a 408 nm (Hoechst 33342) and 488 nm (FD10) laser line, while Cy5-dextran-NG were excited using a 633 nm laser line. Images with different laser lines were taken in rapid succession with a 0.2 s delay. Hoechst 33342 staining was used to image FITC fluorescence at the focal plane of the cell nucleus. Nuclei were detected in the blue channel and used to determine nuclear FITC fluorescence intensity levels in the green channel as previously described, using ImageJ (FIJI, Version 1.8.0) software.

The number of Cy5-dex-NG containing endosomes was manually counted in the red channel (Cy5) using thresholding (applying equal

offset values for each image). Offset values were normalized to the total cell area, which was determined in the green channel based on FITC fluorescence intensity levels using thresholding. The same threshold settings were maintained for each image. The extent of nanogel uptake was measured in the red channel based on red fluorescence intensity values (mean gray value). These endosomal parameters measured were plotted against the respective nuclear FITC levels for each individual cell for a minimum of 50 cells in total. Simple linear regression analysis was performed to investigate the relationship between FITC-dextran delivery (rMFI FITC) and both endosomal parameters using Graphpad Prism software.

Quantification of Cre Recombinase and Granzyme A Delivery in HeLa Cells Using Flow Cytometry: HeLa (reporter) cells were seeded at 1×10^4 cells per well in μ-Slide Angiogenesis Glass Bottom coverslip (ibidi, Munich, Germany). After 24 h, cells were washed twice using PBS. Next, cells were incubated for 2 h in Opti-MEM containing dextran nanogels (dex-NG DS 5.9) together with Cre recombinase (5U) or human recombinant granzyme A (10 μg mL^{-1}) in a total volume of 20 μL. Next, excess dex-NG and protein were washed away using PBS. After 24 h, Cre-recombinase treated reporter cells were visualized using confocal microscopy or analyzed using flow cytometry to determine the percentage of eGFP expressing (eGFP+) cells. The gating strategy used can be found in Figure S11, Supporting Information. One day after granzyme A delivery, HeLa cell viability was measured using the CellTiter-Glo luminescent viability assay. To confirm granzyme A mediated cell death, Annexin V staining was performed according to manufacturer's instructions followed by confocal imaging (408 nm laser line) as previously described.

Nucleofection of HeLa reporter cells was performed using a 4D-nucleofector system and SE Cell Line 4D-Nucleofector X kit S (Lonza Cologne, Germany) following the manufacturer's instructions. Briefly, HeLa reporter cells were trypsinized and 1×10^5 cells were resuspended in nucleofector solution containing Cre recombinase (5U) in a total volume of 20 μL and treated with program CN-114 in 20 μL Nucleocuvette Strips (Lonza Cologne, Germany). After treatment, the cells were washed and transferred to a μ-Slide Angiogenesis Glass Bottom coverslip containing cell culture medium. After 24 h, the cells were harvested for flow cytometry analysis. As a comparison, the commercial reagent PULSin (Polyplus Transfection, Strasbourg, France) was used according to the manufacturer's instructions. Briefly, HeLa reporter cells were seeded at 1.5×10^4 cells per well in a glass bottom 96-well plate (Greiner Bio-One GmbH, Vilvoorde, Belgium). Cre recombinase was complexed at 4 μL PULSin per μg Cre recombinase in a total volume of 20 μL of HEPES buffer (20×10^{-3} M). Next, HeLa reporter cells were washed with PBS and protein-PULSin mix (20 μL) combined with serum-free cell culture medium (80 μL) was added to the cells for 4 h. After 48 h, the cells were harvested for flow cytometry analysis.

Dextran Nanogel-Mediated FITC-Dextran 10 kDa Delivery in Human T Cells: Human T cells were seeded at 1×10^6 cells per well in a glass bottom 96-well plate (Greiner Bio-One GmbH, Vilvoorde, Belgium). Next, cells were washed twice using PBS and incubated in Opti-MEM containing dex-NG DS 5.9 and FD10 (2 mg mL^{-1}) in the presence or absence of N-acetylcysteine (NAC, 10×10^{-3} M). Incubations were performed for 1 h at 37 °C in a humidified atmosphere containing CO$_2$ (5%) unless otherwise specified. Next, nanocarriers and excess proteins were washed away using PBS. After washing, cells were incubated in the presence of TO-PRO-3 iodide (0.5×10^{-6} M) in complete RPMI. Quantitative analysis of delivery efficiency was performed using flow cytometry on living (i.e., TO-PRO-3 negative) cells (CytoFLEX equipped with CytExpert software; Beckman Coulter, Krefeld, Germany). FlowJo software was used for data analysis. The gating strategy is displayed in Figure S11, Supporting Information. For confocal microscopy, human T cell nuclei were stained using Hoechst 33342 and cell viability was confirmed using CellTrace Calcein Red-Orange. Briefly, the cells were washed using PBS and incubated in cell culture medium containing Hoechst 33342 (20 μg mL^{-1}) for 15 min. Finally, staining solution was removed and fresh cell culture medium was added. The cells were kept at 37 °C in humidified atmosphere with CO$_2$ (5%) until confocal imaging. Nucleofection

was performed using a 4D-nucleofector system and P3 Primary Cell 4D-Nucleofector kit (Lonza Cologne, Germany) following manufacturer's instructions. Briefly, 1×10^6 human T cells were resuspended in nucleofector solution containing FD 10 kDa (2 mg mL^{-1}) and treated with program EO-115 (high functionality) in 20 μL Nucleocuvette Strips (Lonza Cologne, Germany). After treatment, cells were washed and transferred to a 96-well plate for further analysis.

Dextran Nanogel-Mediated Gadobutrol Delivery in Human T Cells: Human T cells were seeded at 1×10^6 cells per well in a glass-bottom 96-well plate (Greiner Bio-One GmbH, Vilvoorde, Belgium). Next, cells were washed twice using PBS and incubated in Opti-MEM containing both dex-NG DS 5.9 and gadobutrol (100×10^{-3} M) or gadobutrol (100×10^{-3} M) only. Incubations were performed for 1 h at 37 °C in a humidified atmosphere containing CO$_2$ (5%). Next, nanogels and excess gadobutrol were washed away by large volumes of PBS. Afterwards, 4×10^5 human T cells per condition were resuspended in PBS (25 μL) and transferred to an 18-well, flat μ-Slide (ibidi, Munich, Germany) for further analysis. As a comparison with the current gold standard for cargo delivery in human T cells, gadobutrol was delivered in human T cells using nucleofection as indicated above. Image acquisition was performed by placing each μ-Slide in the cavity of a 50 mL centrifuge tube containing agar (1%, Invitrogen, Merelbeke, Belgium). Next, a horizontal bore 7 T magnet (PharmaScan, Bruker BioSpin, Ettlingen, Germany) with a mouse whole body volume coil (40 mm inner diameter) was used to acquire MR images. An anatomical scan was taken to obtain spatial information using a spin echo RARE sequence with the following parameters: TR/TE (1730/11.1 ms), RARE factor 4, FOV (4 cm × 2.5 cm), matrix (333 × 208), slice thickness (600 μm), 3 averages, acquisition time (3 min 23 s). R_1 relaxometry was performed on a single coronal slice using the following parameters: 10 TRs (8000, 4000, 2000, 1000, 700, 400, 200, 120, 80, 61 ms), TE (11 ms), RARE factor 2, FOV (3 cm × 2 cm), matrix (192 × 128), slice thickness (1 mm), 2 averages, acquisition time (39 min 45 s). Next, R_1 values ($1/T_1$) were calculated using the "evolution" script (ParaVision Version 5.1, Bruker BioSpin, Ettlingen, Germany). The total acquisition time was approximately 40 min.

Statistical Analysis: Statistical analysis was performed using GraphPad Prism software (Version 6). A Student *t*-test was used to compare the mean of 2 conditions. Multiple conditions were compared using a one-way analysis of variance (ANOVA) combined with the post-hoc Tukey test to correct for multiple testing. When comparing several means to a single control mean a post-hoc Dunnett test was applied. Simple linear regression analysis was performed in the same software. Goodness-of-fit was represented as R^2. *P*-values < 0.05 were considered to be statistically significant.

Supporting Information

Supporting Information is available from the Wiley Online Library or from the author.

Acknowledgements

Conflict of Interest

The authors declare no conflict of interest.

Data Availability Statement

The data that support the findings of this study are available from the corresponding author upon reasonable request.

Keywords

[1] M. P. Stewart, R. Langer, K. F. Jensen, *Chem. Rev.* **2018**, *118*, 7409.

[2] M. P. Stewart, A. Sharei, X. Ding, G. Sahay, R. Langer, K. F. Jensen, *Nature* **2016**, *538*, 183.

[3] L. Naldini, *Nat. Rev. Genet.* **2011**, *12*, 301.

[4] A. Tawab, Y. Fan, E. J. Read, R. J. Kurlander, *Transfusion* **2009**, *49*, 536.

[5] X. Ding, M. P. Stewart, A. Sharei, J. C. Weaver, R. S. Langer, K. F. Jensen, *Nat. Biomed. Eng.* **2017**, *1*, 0039.

[6] X. Xu, S. Hou, N. Wattanatorn, F. Wang, Q. Yang, C. Zhao, X. Yu, H. R. Tseng, S. J. Jonas, P. S. Weiss, *ACS Nano* **2018**, *12*, 4503.

[7] A. Aijaz, M. Li, D. Smith, D. Khong, C. Leblon, O. S. Fenton, R. M. Olabisi, S. Libutti, J. Tischfield, M. V. Maus, R. Deans, R. N. Barcia, D. G. Anderson, J. Ritz, R. Preti, B. Parekkadan, *Nat. Biomed. Eng.* **2018**, *2*, 362.

[8] D. Kim, C. H. Kim, J. Il Moon, Y. G. Chung, M. Y. Chang, B. S. Han, S. Ko, E. Yang, K. Y. Cha, R. Lanza, K. S. Kim, *Cell Stem Cell* **2009**, *4*, 472.

[9] L. Warren, P. D. Manos, T. Ahfeldt, Y. H. Loh, H. Li, F. Lau, W. Ebina, P. K. Mandal, Z. D. Smith, A. Meissner, G. Q. Daley, A. S. Brack, J. J. Collins, C. Cowan, T. M. Schlaeger, D. J. Rossi, *Cell Stem Cell* **2010**, *7*, 618.

[10] L. Rohani, C. Fabian, H. Holland, Y. Naaldijk, R. Dressel, H. Löffler-Wirth, H. Binder, A. Arnold, A. Stolzing, *Stem Cell Res.* **2016**, *16*, 662.

[11] S. Rafiq, C. S. Hackett, R. J. Brentjens, *Nat. Rev. Clin. Oncol.* **2020**, *17*, 147.

[12] K. Raemdonck, S. C. De Smedt, *Nat. Biotechnol.* **2015**, *33*, 1026.

[13] T. DiTommaso, J. M. Cole, L. Cassereau, J. A. Buggé, J. L. Sikora Hanson, D. T. Bridgen, B. D. Stokes, S. M. Loughhead, B. A. Beutel, J. B. Gilbert, K. Nussbaum, A. Sorrentino, J. Toggweiler, T. Schmidt, G. Gyuelveszi, H. Bernstein, A. Sharei, *Proc. Natl. Acad. Sci. USA* **2018**, *115*, E10907.

[14] R. Xiong, S. K. Samal, J. Demeester, A. G. Skirtach, S. C. De Smedt, K. Braeckmans, *Adv. Phys. X* **2016**, *1*, 596.

[15] D. Wang, P. W. L. Tai, G. Gao, *Nat. Rev. Drug Discovery* **2019**, *18*, 358.

[16] S. Tong, B. Moyo, C. M. Lee, K. Leong, G. Bao, *Nat. Rev. Mater.* **2019**, *4*, 726.

[17] E. Blanco, H. Shen, M. Ferrari, *Nat. Biotechnol.* **2015**, *33*, 941.

[18] S. Ramishetti, R. Kedmi, M. Goldsmith, F. Leonard, A. G. Sprague, B. Godin, M. Gozin, P. R. Cullis, D. M. Dykxhoorn, D. Peer, *ACS Nano* **2015**, *9*, 6706.

[19] H. Yin, R. L. Kanasty, A. A. Eltoukhy, A. J. Vegas, J. R. Dorkin, D. G. Anderson, *Nat. Rev. Genet.* **2014**, *15*, 541.

[20] D. Peer, J. M. Karp, S. Hong, O. C. Farokhzad, R. Margalit, R. Langer, *Nat. Nanotechnol.* **2007**, *2*, 751.

[21] P. Foroozandeh, A. A. Aziz, *Nanoscale Res. Lett.* **2018**, *13*, 339.

[22] J. Gilleron, W. Querbes, A. Zeigerer, A. Borodovsky, G. Marsico, U. Schubert, K. Manygoats, S. Seifert, C. Andree, M. Stöter, H. Epstein-Barash, L. Zhang, V. Koteliansky, K. Fitzgerald, E. Fava, M. Bickle, Y. Kalaidzidis, A. Akinc, M. Maier, M. Zerial, *Nat. Biotechnol.* **2013**, *31*, 638.

[23] D. Ma, *Nanoscale* **2014**, *6*, 6415.

[24] A. K. Varkouhi, M. Scholte, G. Storm, H. J. Haisma, *J. Controlled Release* **2011**, *151*, 220.

[25] A. Paillard, F. Hindré, C. Vignes-Colombeix, J. P. Benoit, E. Garcion, *Biomaterials* **2010**, *31*, 7542.

[26] T. Van de Vyver, B. Bogaert, L. De Backer, F. Joris, R. Guagliardo, J. Van Hoeck, P. Merckx, S. Van Calenbergh, S. Ramishetti, D. Peer, K. Remaut, S. C. De Smedt, K. Raemdonck, *ACS Nano* **2020**, *14*, 4774.

[27] S. F. Dowdy, *Nat. Biotechnol.* **2017**, *35*, 222.

[28] K. A. Whitehead, R. Langer, D. G. Anderson, *Nat. Rev. Drug Discovery* **2009**, *8*, 129.

[29] S. A. Smith, L. I. Selby, A. P. R. Johnston, G. K. Such, *Bioconjug. Chem.* **2019**, *30*, 263.

[30] H. K. Shete, R. H. Prabhu, V. B. Patravale, *J. Nanosci. Nanotechnol.* **2014**, *14*, 460.

[31] S. K. Samal, M. Dash, S. Van Vlierberghe, D. L. Kaplan, E. Chiellini, C. van Blitterswijk, L. Moroni, P. Dubruel, *Chem. Soc. Rev.* **2012**, *41*, 7147.

[32] F. Marano, S. Hussain, F. Rodrigues-Lima, A. Baeza-Squiban, S. Boland, *Arch. Toxicol.* **2011**, *85*, 733.

[33] A. Panariti, G. Miserocchi, I. Rivolta, *Nanotechnol. Sci. Appl.* **2012**, *5*, 87.

[34] J. Chen, J. A. Hessler, K. Putchakayala, B. K. Panama, D. P. Khan, S. Hong, D. G. Mullen, S. C. DiMaggio, A. Som, G. N. Tew, A. N. Lopatin, J. R. Baker, M. M. B. Holl, B. G. Orr, *J. Phys. Chem. B* **2009**, *113*, 11179.

[35] P. R. Leroueil, S. A. Berry, K. Duthie, G. Han, V. M. Rotello, D. Q. McNerny, J. R. Baker, B. G. Orr, M. M. B. Holl, *Nano Lett.* **2008**, *8*, 420.

[36] S. Hong, P. R. Leroueil, E. K. Janus, J. L. Peters, M. M. Kober, M. T. Islam, B. G. Orr, J. R. Baker, M. M. Banaszak Holl, *Bioconjug. Chem.* **2006**, *17*, 728.

[37] A. Mecke, S. Uppuluri, T. M. Sassanella, D. K. Lee, A. Ramamoorthy, J. R. Baker, B. G. Orr, M. M. Banaszak Holl, *Chem. Phys. Lipids* **2004**, *132*, 3.

[38] S. J. Soenen, L. De Backer, B. Manshian, S. Doak, K. Raemdonck, J. Demeester, K. Braeckmans, S. De Smedt, *Nanomedicine* **2014**, *9*, 61.

[39] R. R. Arvizo, O. R. Miranda, M. A. Thompson, C. M. Pabelick, R. Bhattacharya, J. D. Robertson, V. M. Rotello, Y. S. Prakash, P. Mukherjee, *Nano Lett.* **2010**, *10*, 2543.

[40] B. Wang, L. Zhang, C. B. Sung, S. Granick, *Proc. Natl. Acad. Sci. USA* **2008**, *105*, 18171.

[41] Y. Liu, Z. Zhang, Q. Zhang, G. L. Baker, R. M. Worden, *Biochim. Biophys. Acta – Biomembr.* **2014**, *1838*, 429.

[42] V. V. Ginzburg, S. Balijepalli, *Nano Lett.* **2007**, *7*, 3716.

[43] S. Hong, A. U. Bielinska, A. Mecke, B. Keszler, J. L. Beals, X. Shi, L. Balogh, B. G. Orr, J. R. Baker, M. M. Banaszak Holl, *Bioconjug. Chem.* **2004**, *15*, 774.

[44] S. Li, N. Malmstadt, *Soft Matter* **2013**, *9*, 4969.

[45] J. Lin, A. Alexander-Katz, *ACS Nano* **2013**, *7*, 10799.

[46] D. Fischer, Y. Li, B. Ahlemeyer, J. Krieglstein, T. Kissel, *Biomaterials* **2003**, *24*, 1121.

[47] K. Raemdonck, B. Naeye, K. Buyens, R. E. Vandenbroucke, A. Høgset, J. Demeester, S. C. D. Smedt, *Adv. Funct. Mater.* **2009**, *19*, 1406.

[48] S. hee Kim, C. C. Chu, *J. Biomed. Mater. Res.* **2000**, *53*, 258.

[49] K. Raemdonck, T. G. Van Thienen, R. E. Vandenbroucke, N. N. Sanders, J. Demeester, S. C. De Smedt, *Adv. Funct. Mater.* **2008**, *18*, 993.

[50] R. J. H. Stenekes, S. C. De Smedt, J. Demeester, G. Sun, Z. Zhang, W. E. Hennink, *Biomacromolecules* **2000**, *1*, 696.

[51] S. R. Van Tomme, W. E. Hennink, *Expert Rev. Med. Devices* **2007**, *4*, 147.

[52] W. B. Liechty, R. L. Scheuerle, J. E. Vela Ramirez, N. A. Peppas, *Bioeng. Transl. Med.* **2019**, *4*, 17.

[53] S. Patil, A. Sandberg, E. Heckert, W. Self, S. Seal, *Biomaterials* **2007**, *28*, 4600.

[54] C. C. Chen, T. H. Tsai, Z. R. Huang, J. Y. Fang, *Eur. J. Pharm. Biopharm.* **2010**, *74*, 474.

[55] C. J. De Groot, M. J. A. Van Luyn, W. N. E. Van Dijk-Wolthuis, J. A. Cadée, J. A. Plantinga, W. Den Otter, W. E. Hennink, *Biomaterials* **2001**, *22*, 1197.

[56] W. E. Hennink, C. F. Van Nostrum, *Adv. Drug Delivery Rev.* **2002**, *54*, 13.

[57] K. Raemdonck, B. Naeye, A. Høgset, J. Demeester, S. C. De Smedt, *J. Controlled Release* **2010**, *145*, 281.

[58] R. Xiong, R. E. Vandenbroucke, K. Broos, T. Brans, E. Van Wonterghem, C. Libert, J. Demeester, S. C. De Smedt, K. Braeckmans, *Nat. Commun.* **2016**, *7*, 12982.

[59] J. Rejman, V. Oberle, I. S. Zuhorn, D. Hoekstra, *Biochem. J.* **2004**, *377*, 159.

[60] I. S. Zuhorn, R. Kalicharan, D. Hoekstra, *J. Biol. Chem.* **2002**, *277*, 18021.

[61] W. T. Godbey, K. K. Wu, A. G. Mikos, *Proc. Natl. Acad. Sci. USA* **1999**, *96*, 5177.

[62] P. Li, Y. F. Poon, W. Li, H. Y. Zhu, S. H. Yeap, Y. Cao, X. Qi, C. Zhou, M. Lamrani, R. W. Beuerman, E. T. Kang, Y. Mu, C. M. Li, M. W. Chang, S. S. Jan Leong, M. B. Chan-Park, *Nat. Mater.* **2011**, *10*, 149.

[63] O. Ebert, S. Finke, A. Salahi, M. Herrmann, B. Trojaneck, P. Lefterova, E. Wagner, R. Kircheis, D. Huhn, F. Schriever, I. G. H. Schmidt-Wolf, *Gene Ther.* **1997**, *4*, 296.

[64] S. Mizrahy, I. Hazan-Halevy, N. Dammes, D. Landesman-Milo, D. Peer, *Mol. Ther.* **2017**, *25*, 1491.

[65] J. Shi, Y. Ma, J. Zhu, Y. Chen, Y. Sun, Y. Yao, Z. Yang, J. Xie, *Molecules* **2018**, *23*, 3044.

[66] T. Kotnik, P. Kramar, G. Pucihar, D. Miklavčič, M. Tarek, *IEEE Electr. Insul. Mag.* **2012**, *28*, 14.

[67] I. Minn, S. P. Rowe, M. G. Pomper, *Lancet Oncol.* **2019**, *20*, e443.

[68] A. Mantei, S. Rutz, M. Janke, D. Kirchhoff, U. Jung, V. Patzel, U. Vogel, T. Rudel, I. Andreou, M. Weber, A. Scheffold, *Eur. J. Immunol.* **2008**, *38*, 2616.

[69] V. Mokhtari, P. Afsharian, M. Shahhoseini, S. M. Kalantar, A. Moini, *Cell J.* **2017**, *19*, 11.

[70] M. J. Scheffel, G. Scurti, M. M. Wyatt, E. Garrett-Mayer, C. M. Paulos, M. I. Nishimura, C. Voelkel-Johnson, *Cancer Immunol. Immunother.* **2018**, *67*, 691.

[71] M. J. Scheffel, G. Scurti, P. Simms, E. Garrett-Mayer, S. Mehrotra, M. I. Nishimura, C. Voelkel-Johnson, *Cancer Res.* **2016**, *76*, 6006.

[72] I. Van Audenhove, J. Gettemans, *EBioMedicine* **2016**, *8*, 40.

[73] G. Meinke, A. Bohm, J. Hauber, M. T. Pisabarro, F. Buchholz, *Chem. Rev.* **2016**, *116*, 12785.

[74] L. J. Scott, *Clin. Drug Investig.* **2018**, *38*, 773.

[75] A. J. Managh, S. L. Edwards, A. Bushell, K. J. Wood, E. K. Geissler, J. A. Hutchinson, R. W. Hutchinson, H. J. Reid, B. L. Sharp, *Anal. Chem.* **2013**, *85*, 10627.

[76] E. Terreno, S. G. Crich, S. Belfiore, L. Biancone, C. Cabella, G. Esposito, A. D. Manazza, S. Aime, *Magn. Reson. Med.* **2006**, *55*, 491.

[77] E. Di Gregorio, G. Ferrauto, E. Gianolio, S. Aime, *Contrast Media Mol. Imaging* **2013**, *8*, 475.

[78] O. G. de Jong, D. E. Murphy, I. Mäger, E. Willms, A. Garcia-Guerra, J. J. Gitz-Francois, J. Lefferts, D. Gupta, S. C. Steenbeek, J. van Rheenen, S. El Andaloussi, R. M. Schiffelers, M. J. A. Wood, P. Vader, *Nat. Commun.* **2020**, *11*, 1113.